

The University of Maine

DigitalCommons@UMaine

Electronic Theses and Dissertations

Fogler Library

Summer 8-23-2019

Performance of the Intrac Wireless Activity Tracking System for the Afari Assistive Device

Drew Browning

University of Maine, drew.browning@maine.edu

Follow this and additional works at: <https://digitalcommons.library.umaine.edu/etd>

Recommended Citation

Browning, Drew, "Performance of the Intrac Wireless Activity Tracking System for the Afari Assistive Device" (2019). *Electronic Theses and Dissertations*. 3091.

<https://digitalcommons.library.umaine.edu/etd/3091>

This Open-Access Thesis is brought to you for free and open access by DigitalCommons@UMaine. It has been accepted for inclusion in Electronic Theses and Dissertations by an authorized administrator of DigitalCommons@UMaine. For more information, please contact um.library.technical.services@maine.edu.

**PERFORMANCE OF THE INTRAC WIRELESS ACTIVITY TRACKING SYSTEM FOR THE AFARI
ASSISTIVE DEVICE**

By

Drew Browning

B.S. Boston University, 2014

A THESIS

Submitted in Partial Fulfillment of the

Requirements for the Degree of

Master of Science

(in Mechanical Engineering)

The Graduate School

The University of Maine

August 2019

Advisory Committee:

Dr. Vincent Caccese, Professor of Mechanical Engineering, Advisor

Dr. Babak Hejrati, Professor of Mechanical Engineering, Co-Advisor

Dr. Elizabeth Depoy, Professor of Social Work and Interdisciplinary Disability Studies

PERFORMANCE OF THE INTRAC WIRELESS ACTIVITY TRACKING SYSTEM FOR THE AFARI ASSISTIVE DEVICE

By Drew Browning
Thesis advisor: Vince Caccese

An Abstract of the Thesis Presented
in Partial Fulfillment of the Requirements for the
Degree of Master of Science
(in Mechanical Engineering)
August 2019

Afari is a mobility device that was designed to be more recreational, aesthetic, and functional outside than the typical mobility devices commonly used today such as walkers, crutches, and rollators. The Afari transfers weight from a user through the arm rests and enforces an upright posture while walking with correct adjustments to the arm rest height.

In addition to assisting with walking or running, a sensor system fitted to the Afari device has been designed to analyze different aspects of activity tracking such as the dynamic loading applied to the arm rests, spatial-temporal gait parameters, speed, and distance. This includes various sensors, namely, load cells for each arm rest, an inertial measurement unit, and a speed and distance sensor that wirelessly transmit data via Bluetooth Low Energy (BLE) to either a smartphone or computer. The total distance, pitch angle, right and left loading on each armrest can be viewed in real time by the user. An algorithm was created in MATLAB to process all the raw data and compute cadence, stride length, average toe-off and heel strike angle,

swing and stance time, and speed over the duration of active use. An Afari user can monitor these different aspects of their activity and adjust accordingly to potentially improve their balance or gait.

TABLE OF CONTENTS

LIST OF TABLES.....	v
LIST OF FIGURES.....	vi
CHAPTER	
1. INTRODUCTION.....	1
1.1. Background.....	1
1.2. Description of the Afari Assistive Device.....	4
1.2.1. The INTRAC Sensing System.....	5
1.3. Activity Tracking Systems.....	8
1.4. Assistive Device Activity Tracking Systems.....	11
1.5. Available Sensors for Activity Tracking	14
1.5.1. Commercial off the Shelf Sensor Devices.....	15
1.5.2. Inertial Measurement Units.....	18
1.5.3. Force Measurement Devices.....	20
1.6. IMU Processing Algorithms.....	22
1.7. Desired Gait Measurements.....	22
1.8. Project Objectives and Scope.....	26

2.	INTRAC MONITORING SYSTEM FOR AFARI.....	27
2.1.	Overview of the INTRAC System.....	27
2.1.1.	Weight Measurement Module.....	28
2.1.2.	Speed/Distance Measurement Module.....	29
2.1.3.	Ankle or Shoe mounted Inertial Measurement Units.....	29
2.1.4.	Foot Pressure Measurement Unit.....	30
2.2.	Electronics and Software.....	31
2.3.	Arm Rest Load Cell Design	32
2.3.1.	Load Cell Calibration.....	34
2.3.2.	Load Cell Calibration Results.....	37
2.3.3.	Dependence on Position of Weight.....	38
2.3.4.	Dependence on Battery Life.....	39
2.4.	Inertial Measurement Unit Design.....	41
2.4.1.	Inertial Measurement Unit Calibration.....	43
2.4.2.	Inertial Measurement Unit Verification Test.....	44
2.5.	Speed and Distance Sensor Design.....	47
2.5.1.	Speed and Distance Sensor Calibration.....	49
3.	SYSTEM TESTING.....	50

3.1. Testing Conditions and Setting.....	50
3.2. Speed and Distance Procedure.....	51
3.2.1. Speed and Distance Sensor Results.....	51
3.3. Load Cell Monitoring System Procedure.....	53
3.3.1. Load Cell Monitoring System Results.....	54
3.4. Inertial Measurement Unit Procedure.....	56
3.4.1. Inertial Measurement Unit Results.....	57
3.5. TekScan Procedure.....	59
3.5.1. TekScan Hardware Setup.....	61
3.5.2. TekScan Results.....	62
3.6. Force Sensor Testing Procedure.....	63
3.6.1. Force Sensor Results.....	65
3.7. Data Acquisition Device.....	69
3.8. System Performance Evaluation.....	69
4. SUMMARY AND CONCLUSION.....	74
REFERENCES.....	76
APPENDIX.....	79
BIOGRAPHY OF THE AUTHOR.....	82

LIST OF TABLES

Table 1.1	Summary of the IMUs Considered for Use	19
Table 2.1	Current Features of INTRAC.....	25
Table 2.2	Distance Recorded	37
Table 3.1	Gait and Balance Parameters.....	55

LIST OF FIGURES

Figure 1.1	The Afari Assistive Device	3
Figure 1.2	Diagram showing the undesired posture of walker users.	4
Figure 1.3	Afari handlebars with load cells attached	6
Figure 1.4	INTRAC overview of Afari use (a) and close-up of the IMU device (b)	7
Figure 1.5	IMU placement on shank in the saggital plane (Sijobert, et al, 2015).....	9
Figure 1.6	Graph of angular velocity (deg/seconds) against time (seconds) (Sijobert et al, 2015)	10
Figure 1.7	Placement of IMUs (Vargas, 2016)	11
Figure 1.8	i-Walker mobility device (Cortés, et al, 2008)	12
Figure 1.9	Smart walker fitted with sensors and CPU (Jiménez et al, 2018)	13
Figure 1.10	Yostlabs Bluetooth device (yostlabs.com)	17
Figure 1.11	MetaMotionR device and phone application (MMR).....	17
Figure 1.12	Adafruit FXOS8700 Breakout IMU on the left (a) Sparkfun IMU Breakout MPU-9250 on the right (b). (adafruit.com) (sparkfun.com)	18
Figure 1.13	Adafruit BNO055 Breakout IMU (adafruit.com)	19
Figure 1.14	Typical load cell based on strain gauge (TekScan).....	20
Figure 1.15	Diagram of Wheatstone bridge where R is the resistance (Strain Gauges).....	21

Figure 1.16 TekScan force sensitive resistor	21
Figure 1.17 Normal gait cycle with characteristic points of the right foot (Sijobert, et al, 2015)	23
Figure 1.18 Trajectories of the knee adduction moment (N*m) are shown for four participants with different toe-out angles shown on lower right (Chang, 2007).....	25
Figure 2.1 INTRAC System Design Overview.....	28
Figure 2.2 Ankle strapped and shoe clip IMU	30
Figure 2.3 Foot sensor mold and prototype	31
Figure 2.4 a) Load cell monitoring system with all components b) other side of breadboard c) aluminum interface with strain gauge attached.	33
Figure 2.5 Weight monitoring system's placement on the Afari.....	34
Figure 2.6 Calibration setup for Afari weight bearing monitoring system	35
Figure 2.7 Load cell calibration user interface.....	36
Figure 2.8 Weight (lb) with respect to time (s) for left load cell calibration	37
Figure 2.9 Weight (lb) with respect to time (s) for right load cell calibration	38
Figure 2.10 Weight dependence positions	38
Figure 2.11 Weight (lb) with respect to the AD count for the left load cell	39
Figure 2.12 Load cell battery's voltage (V) with respect to time (minutes)	40
Figure 2.13 Weight (lb) with respect to AD count of different battery voltages	41

Figure 2.14 Wiring and components of the IMU device.....	42
Figure 2.15 IMU case with clip attached.....	
Figure 2.16 Placement of IMU and optical markers	45
Figure 2.17 Displacement of the heel marker (in) on the left axis and the foot to floor angle (deg) on the right axis with respect to time (s).....	46
Figure 2.18 Internal components of speed and distance sensor.....	47
Figure 2.19 Reed switch function	48
Figure 2.20 Placement of magnets on wheel	49
Figure 3.1 Parking lot setting during Afari use.....	50
Figure 3.2 Distance (ft) travelled with respect to time (s) for no unweighting.....	51
Figure 3.3 Distance (ft) travelled with respect to time (s) for 25% unweighting	52
Figure 3.4 Distance (ft) travelled with respect to time (s) for 50% unweighting.....	52
Figure 3.5 Force (lb) applied to arm rests with respect to time (s) for no unweighting	54
Figure 3.6 Force (lb) applied to arm rests with respect to time (s) for 25% unweighting	55
Figure 3.7 Force (lb) applied to arm rests with respect to time (s) for 50% unweighting (a) 180 second trial (b) 30 second trial.....	56
Figure 3.8 IMU position for Afari use.....	56

Figure 3.9 Graph of foot to floor angle (deg) with respect to time (s) for no unweighting	57
Figure 3.10 Graph of foot to floor angle (deg) with respect to time (s) for 25% unweighting	58
Figure 3.11 Graph of foot to floor angle (deg) with respect to time (s) for 50% unweighting (a) 180 second trial (b) 30 second trial	58
Figure 3.12 Graph of pitch angle (deg) with respect to time (s) of one stride cycle	59
Figure 3.13 TekScan foot pressure sensor	60
Figure 3.14 Wiring and components of the IMU device.....	60
Figure 3.15 TekScan sensor system set-up (F-Scan User Manual)	61
Figure 3.16 Force (lb) of each foot with respect to time (s) while walking.....	62
Figure 3.17 Four separate force sensors and one capacitive sensor on the far right	63
Figure 3.18 Testing set-up for calibration of force sensors	64
Figure 3.19 Interaction between the force sensor and clamp area	65
Figure 3.20 AD count with respect to applied force (lb) for Mouser Electronic rectangular FSR	65
Figure 3.21 AD count with respect to applied force (lb) for Mouser Electronic circular FSR.....	66

Figure 3.22 AD count with respect to applied force (lb) for TekScan large FSR	66
Figure 3.23 AD count with respect to applied force (lb) for TekScan small FSR	67
Figure 3.24 AD count with respect to applied force (lb) for SingleTact capacitive sensor.....	67
Figure 3.25 AD count with respect to applied force (pounds) for loading and unloading of the three different sensors labelled	68
Figure 3.26 User interface of Afari application before being connected to devices; Step 1 Connect, Step 2 Start	70
Figure 3.27 User interface of Afari application while being connected to all sensors; Step 3 Stop, Step 4 e-mail	71

CHAPTER 1

INTRODUCTION

Over 6.1 million older adult community residents in the US use assistive devices such as canes, crutches, and walkers to help them with mobility (University of California, 2015). These devices are primarily prescribed to people to reduce the risk of falling, which is the leading cause of death from injury among older adults. However, 30-50% of this population have been abandoning these devices due to difficulty of use, stooped posture, pain, injuries, and the stigma of being perceived as crippled (Gell et al, 2015). Many of these older adults are also limited by their devices to go outside and it has been shown that simply being outdoors can “enhance healthy sleep patterns, reduce depression, improve cardiac health and cognition” (Resnik et al, 2009). Therefore, a device which could eliminate primary reasons of abandonment as with the standard walkers and functions effectively outside would be ideal for people in need of mobility equipment.

1.1 Background

Activity monitoring is a critically important aspect of health care, particularly when detecting changes in a person’s biomechanics can be used to avoid the risk of deterioration and an impending health threatening event. Gait analysis is important for monitoring how diseases such as Alzheimer’s and Parkinson’s affect motor skills as well as gauging the recovery of a person with a lower extremity injury. However, clinical gait testing has not been that common due to cost, \$300,000 to \$500,000 for equipping a clinical gait laboratory, and the time required for testing which sometimes yielded unreliable results (Zheng et al, 2014). There is a need for

gait testing that has more accessibility, affordability, and reliability so gait testing is used more commonly for monitoring diseases that affect gait as well as assessing the recovery from a lower body injury. A gait tracking device that allows for daily self-diagnosis of gait and balance would be convenient as the user could avoid making a doctor's trip each time costing them time and money. Furthermore, the user could see their activity progression immediately which may give them more incentive to continue exercising and improve their health daily. If the user notices regression in their balance and gait from the self-diagnosis they can take appropriate measures to mitigate the risk of falling and injuries.

There are other aspects of activity tracking and their importance will vary depending on the subject's needs. Cardiovascular health could be a concern and there are affordable devices that can track heart rate during exercise. Tracking the heart rate could be important to ensure a subject doesn't pass a threshold that could potentially lead to a heart attack. Posture while walking or running is another trait that may be monitored to avoid poor form which can lead to back problems. Muscle activity can be tracked with electromyography which uses surface or intramuscular electrodes to measure the current produced by the contractions of muscles. Tracking muscle activity can be beneficial for verifying that specific muscles are working as they should for certain actions. Ground reaction forces can also be tracked to determine body weight distribution or body sway and when used in combination with video measurements the torque, work and power at each joint can be calculated (Western et al, 2013).

1.2 Description of the Afari Assistive Device

The Afari, shown in Figure 1.1, was developed at the University of Maine in cooperation with Mobility Technologies of Brunswick, ME. It was created by Drs. Elizabeth DePoy and Steven Gilson to address an unmet need for a device that functions more recreationally and is aesthetic. Its objective is to address some of the problems associated with standard walkers and was designed to operate effectively on outside terrain. The standard walker problems include difficulty to maintain upright posture, requirement of the user to pick up the equipment to advance incrementally, inability to run with device, and induced strains in the upper body. The target population is people with poor balance or gait due to lower body weakness, diseases, or conditions that affect gait or balance.



Figure 1.1: The Afari Assistive Device

The Afari has several advantages over other assistive devices due to its design features. One advantage is it allows for more upright posture as the handlebars are adjustable to fit the

subject's height as opposed to the hunched-over posture observed with users of standard walkers shown in Figure 1.2.



Figure 1.2: Diagram showing the undesired posture of walker users.
(mayoclinic.org)

Mayo Clinic advises walker users to stay upright as they move with the walker, push the walker not too far in front of them and to take small steps moving slowly when turning (mayoclinic.org, 2016). Instead of carefully moving in increments as with a standard walker, Afari users will move continuously maintaining an upright posture. Furthermore, an Afari user can take large steps and move faster keeping an upright posture because the user is moving with the assistive device as opposed to pushing it. This allows Afari users to walk more naturally, so the transition to moving without a device is easier. At the least, the Afari users maintain their current gait whereas walker users must generally change their gait while moving with the walker.

There is a risk of falling with the standard walker when the walker is lifted and moved forward compromising stability and requires adequate upper body strength. The Afari addresses this

problem by keeping contact with the ground during use so stability stays constant potentially reducing the risk of falling. This allows the user to focus more on walking or running without the periodic loss of stability.

Another advantage of the Afari is a potentially safer and steadier navigation at varying speeds. Most walkers lack an active steering mechanism and properly functioning braking system which gives the user more control, reducing the risk of falling. The disc braking system on the Afari is effective and easy to engage as minimal hand grip force is required. Afari offers extra stability and ergonomics as it is fitted with arm rests which improve unweighting and remove direct impact on the wrist, elbow, and shoulder joints.

There is a stigma associated with walkers and many people want to avoid the “crippled” label. The Afari has a different look from the standard walker and could be considered as an exercise device as opposed to a medical device which may give the subject’s more confidence and make them more apt to use it around people. Furthermore, as the Afari capable of traversing most terrains an Afari user could exercise with it in quiet areas out of the public eye if that is a concern. Afari’s ability to be used almost anywhere distinguishes it from most other mobility devices that are designed to move on flat surfaces. Research has shown that being outside can enhance healthy sleep patterns, counter depression, and limit cognitive deterioration (Resnik et al, 2009).

1.2.1 The INTRAC Sensing System

A sensing system called INTRAC™ is being developed to monitor the use of the Afari device in real time. This system is composed of multiple sensors which were desired to be non-invasive

and give valuable feedback on weight bearing, speed, distance, gait and balance. A load cell has been implemented in each arm rest, shown in Figure 1.3, which measures the weight bearing force applied through the forearms. The load cell device is Bluetooth Low Energy (BLE) compatible and can send data directly to a subject's smartphone with the INTRACTM application, so they can see their weight distribution in real time or record while walking with Afari and see the weight distribution over time. This can be useful information for subjects undergoing rehabilitation as their goal is to become more comfortable applying less force through their forearms until it no longer becomes necessary to use the unweighting ability of the Afari. However, some subjects have conditions that will not improve that significantly and may need to continue to use the Afari to exercise.



Figure 1.3: Afari handlebars with load cells attached.

Additional sensors have been incorporated with the system to give more information to the Afari user about their activity and gait. The speed and distance sensor, also known as a Hall

sensor, measures distance traveled and speed in real time by counting each time a magnet passes and this is placed on the wheel of the Afari shown in Figure 1.4. The final sensor fitted to the Afari is an inertial measurement unit (IMU). The IMU can sense acceleration, angular velocity and magnetic field which through a sensor fusion algorithm allows for the measurement of stride length/distance between steps, and the number of steps of the Afari user. The IMU is the only sensor not fitted to the Afari but rather can be used as a stand-alone device that can be attached to the user's shoe with a clip. All the data received from these sensors can be seen on the INTRAC phone app simultaneously. Further details of this system will be given in Section 2.4.

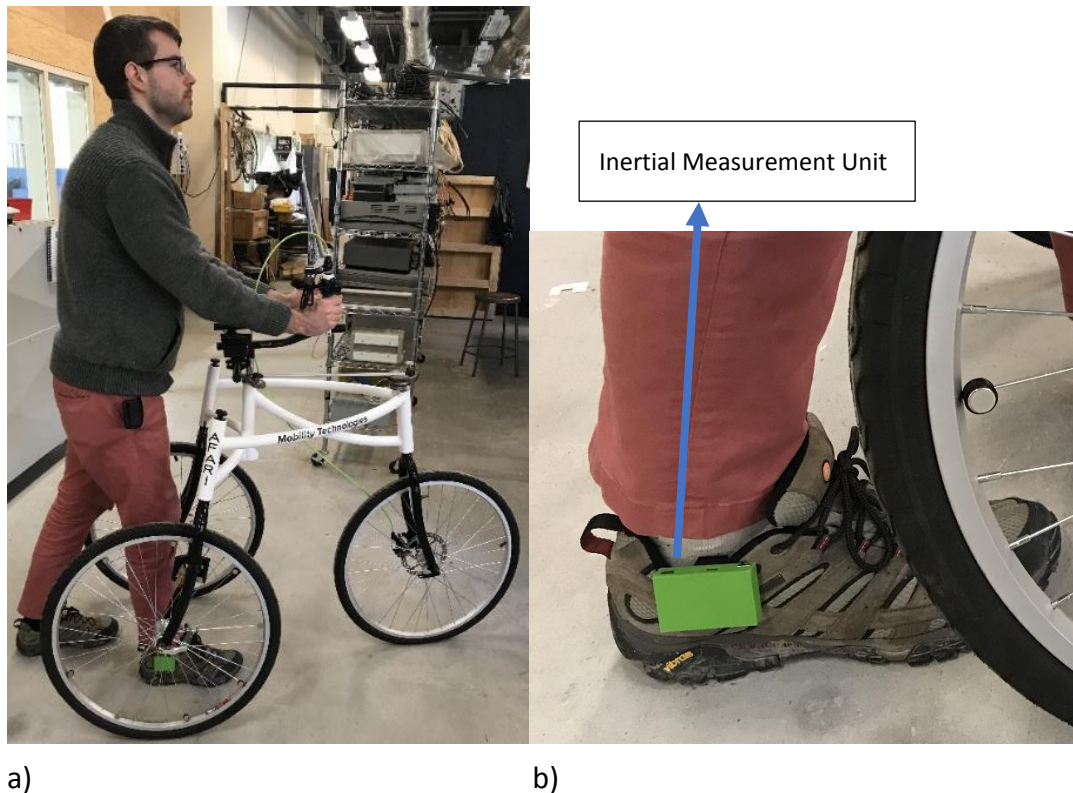


Figure 1.4: INTRAC overview of Afari use (a) and close-up of the IMU device (b)

1.3 Activity Tracking Systems

The most commonly used research and clinical method for biomechanical gait analysis is an optical motion capture system with high-speed cameras and infrared markers. A study performed by Vette (2018) used an 8-camera, optoelectronic motion capture system to collect three-dimensional bilateral kinematic data of the subject's foot to track the foot to floor angle. A toe marker was placed between subject's second and third metatarsal heads of each foot and the heel marker was placed level with the toe marker on the midline (Vette, 2018). The motion capture system tracks the segment between the markers and record the angle of foot to floor at 60 Hz. This study was specific in only measuring the foot dynamics but usually the camera motion capture system is used to record full body motion placing markers over the subject's entire body as it is easy to incorporate additional markers. The motion capture system is limited in its adaptability for use in different environments because it is difficult to move and set up, sensitive to light and obstacles. Accordingly, it is only applicable to laboratory and clinical settings.

Wearable sensors present advantages of lower cost, higher flexibility, portability and adaptability. There are many studies that placed IMUs on a subject's body to capture their motion for gait and balance analysis (Vargas et al, 2016) (Li et al, 2016) (Postolache et al, 2015) (Shenggao et al, 2012) (Sjobert et al, 2015). Depending on the desired gait information, the position of the IMU can vary from feet, legs, back, or chest. The most common placement is the ankle or shank to measure the foot to floor angle to determine gait characteristics such as heel strike, stride length, and cadence. A study (Sijobert et al, 2015) implemented an IMU placing it on the subject's shank as shown in Figure 1.5.

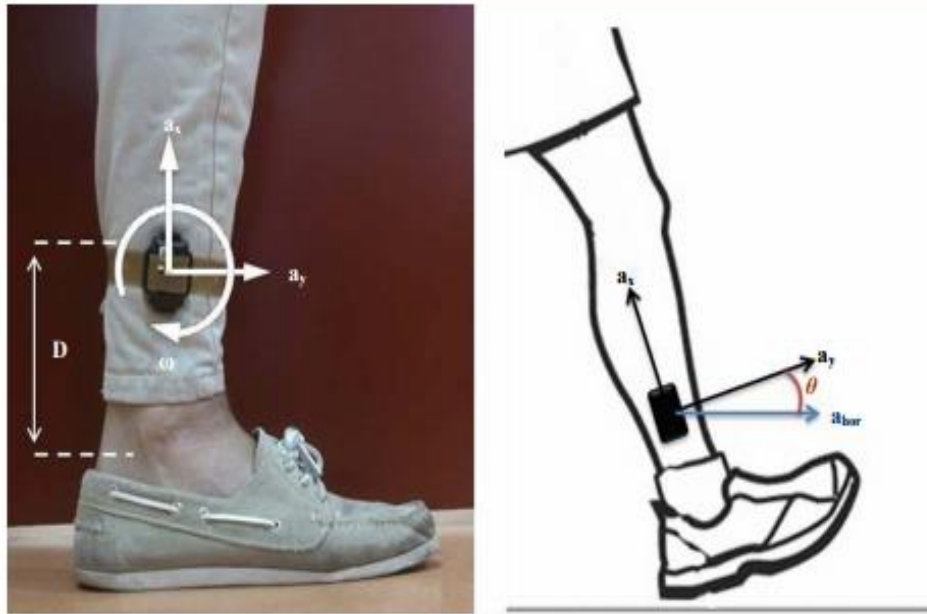


Figure 1.5: IMU placed on the shank in the sagittal plane (Sijobert, et al, 2015)

The IMU was used to retrieve the angular velocity while walking to determine the heel-strike and toe-off instances. These instances correspond to the negative impulses in the angular velocity and an algorithm was created to detect these points shown in Figure 1.6 “through a series of time-varying thresholds combined with a sliding window technique” (Sijobert et al, 2015).

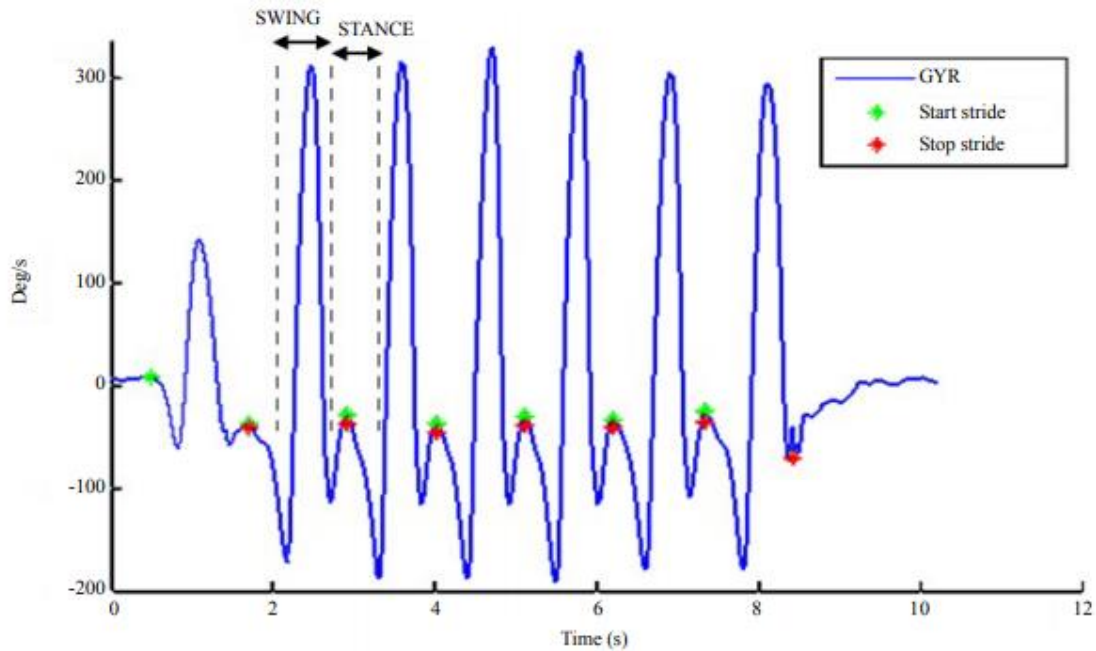


Figure 1.6: Graph of angular velocity (deg/seconds) with respect to time (seconds)

(Sijobert et al, 2015).

Using these gait cycle characteristics other gait parameters were calculated including cadence, stride length, and stride regularity. This study also focused on gait symmetry because while working with patients at a hospital they observed “many patients have difficulty in holding gait balance: because of physical impairment or lack of confidence, they tend to put more weight of the body on one foot than on another, leading to asymmetric gait patterns (Sijobert et al, 2015). To quantify a subject’s gait symmetry, the velocity of both feet were measured and compared to determine the subject’s gait balance as legs moving at different speeds results in gait asymmetry.

One study (Vargas et al, 2016) used multiple inertial measurement units or IMUs to capture lower body motion and their placement is shown in Figure 1.7.

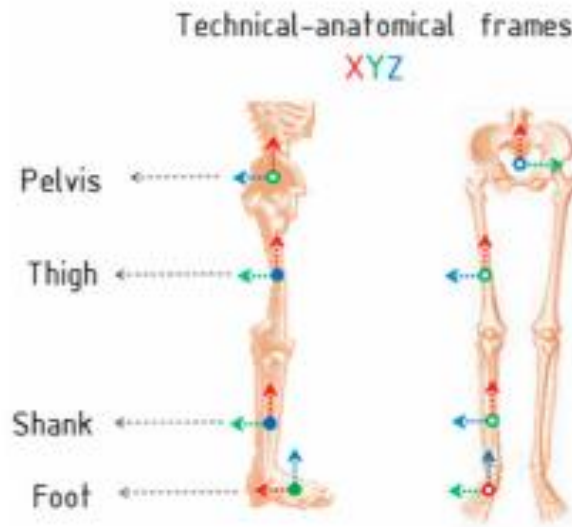


Figure 1.7: Placement of IMUs (Vargas, 2016)

This study used a calibration algorithm to define the orientations of the technical-anatomical frames in order to calculate accurate joint angles. Results from this study “indicate that the method is suitable to measure tridimensional angles of the hip, knee and ankle of the humans’ joints during free walking” (Vargas et al, 2016).

1.4 Assistive Device Activity Tracking Systems

There are several assistive devices that are incorporated with an activity tracking system. There are assistive devices with passive activity tracking or other devices that assume some control and actively guide the user with activity tracking feedback.

An example of the latter is the i-Walker, shown in Figure 1.8, is a rollator with four wheels and two degrees of freedom with two wheels placed closest to the user fixed, driven by independent motors embodied in the hub of the wheel.



Figure 1.8: i-Walker mobility device (Cortés, et al, 2008)

This assistive device has force sensors on the handlebars to measure the interaction force of the user. There are force sensors located on rear wheels for measuring the normal force exerted by the floor on the wheels for detecting overturn risk (Cortés, et al, 2008). There are also encoders on each wheel to measure distance and an inclinometer to detect inclined surfaces. Using the feedback from all these sensors “to validate the motor torques strategies and measure the user’s reactions to them in addition to their behavior” the i-Walker can “modify the user’s behavior and his/her perception of the followed path” (Cortés, et al, 2008). The i-Walker “monitors the users to see if they are resisting the actions (steering/braking) selected by the walker. If they are, the movements are adjusted. This cycle continues until the user agrees with the motion (i.e. does not resist it) or manually over-rides it. This interaction forms the basis of the feedback loop between user and agent (Cortés, et al, 2008)”.

Another similar mobility device developed by Jiménez et al actively guides the user along a predetermined path with an integrated controller is shown in Figure 1.9.



Figure 1.9: Smart walker fitted with multiple sensors and CPU
(Jiménez et al, 2018)

To retrieve information for obstacle detecting, a RP-LIDAR laser sensor is integrated into the smart walker. The robot's position and orientation is captured in real-time by measuring the wheel velocities with optical shaft encoders and an inertial measurement unit (Jiménez et al, 2018). This smart walker has force sensors under each forearm supporting platform to determine the user's motion intentions. A laser rangefinder sensor is used to obtain the distance between the user's legs and the walker to avoid collisions between the user and walker. Furthermore, a computer is embedded for control and processing tasks.

A smart walker with a passive activity tracking system was developed by Yasin et al (2016). This device was designed specifically for improving the efficiency of physiotherapists by allowing them monitor patients remotely. This smart walker is foldable and includes a retractable seat for users that allows the user to sit but still push themselves along while using the device. This device has sensors integrated that can detect falls, record duration of sitting, and measure distance travelled. Sitting is detected a force resistive sensor embedded in the seat cover. An accelerometer measures the tilt of the device and if it exceeds a preset threshold a notification will be sent to the telecommunication device. Distance travelled is measured with a Hall Effect sensor which counts each wheel rotation. This smart walker incorporated a wireless telecommunication device, Zigbee, to transmit the information of the patient's progress during the session (Yasin et al, 2016).

Another study (Postolache et al, 2015) used a combination MEMs, IMU, and microwave Doppler radars as a passive activity tracking system for physical rehabilitation with walkers and rollators. A set of Doppler radar arrays were attached to a rollator to capture the motion of the user's legs unobtrusively. The acquisition of the signals from the Doppler radar sensors was transmitted from a "multifunction board NI MyDAQ to the embedded PC mounted also on the rollator" (Postolache et al, 2015). Furthermore, a separate IMU wireless network was implemented, placing the IMUs on top of each foot, for additional gait information.

1.5 Available Sensors for Activity Tracking

Literature was researched to assess certain sensors and methods that would best capture a subject's gait and other biomechanical parameters while using the Afari. The focus was on low cost, low profile devices that could be deployed for the Afari. This section briefly summarizes

some of the sensor types and systems deemed viable. Consideration was given to package size, ease of implementing into the INTRAC system, power consumption and cost.

1.5.1 Commercial off the Shelf Sensor Devices

Using a phone as a sensor was the first device considered. Ellis et al. (2015) stated that smartphones offer potential benefits in terms of cost savings, portability, customizability, patient tolerance, and deployment scalability for use as a sensor system. While these strengths cannot be ignored the phone being used as both the sensor and as the data acquisition device can be problematic. The position of the sensor is crucial as its orientation needs to be stable and it would be difficult to ensure this while using the phone simultaneously. Nevertheless, Sun, Bing, et al (2014) were able to analyze gait characteristics from an iPhone's embedded tri-axial accelerometer and gyrometer while the phone was in a subject's right and left pants pockets and center of the lower back area. These gait characteristics include "gait frequency, symmetry coefficient, dynamic range and similarity coefficient of characteristic curves" (Sun, Bing, et al, 2014). They accomplished this by using a fourth-order Runge-Kutta algorithm and quaternion to combine inertial data, solve linear acceleration and eliminate the errors caused by attitude change and gravitational acceleration (Sun, Bing, et al, 2014). An alternative could be using a separate sensor connected to the phone through Bluetooth communication so a subject could see their gait characteristics and other biomedical parameters in real time with their phone.

Another existing activity tracking device that was considered was the FitBit. To date, this device was shown to have some major flaws with accuracy and reliability of biomechanical

measurements (Fortune, 2014, Resnick, 2009). Fortune (2014) documented the discrepancy between the step counts measured by the Fitbit and concluded that the Fitbit step counts were significantly lower compared to steps that were counted manually based on the video recordings.

Resnick (2009) echoed these findings and stated that Fitbit “didn’t detect steps for velocities less than 0.5 m/s when located on the waist and detected only approximately 50% of steps for velocities less than 0.5 m/s and greater than 2 m/s when located on the ankle.” These flaws with the FitBit make it inadequate for use with the Afari because subjects will typically be moving at slower speeds, below 0.5 m/s, during Afari’s use when starting and stopping. Furthermore, some subjects that are more athletic may want to run with Afari as well which could exceed 2 m/s.

A more sophisticated and reliable device was discovered called 3-Space from YostLabs shown in Figure 1.10. This device “uses triaxial gyroscope, accelerometer, and compass sensors in conjunction with advanced processing and on-board quaternion-based orientation filtering algorithms to determine orientation relative to an absolute reference in real-time” (yostlabs.com). However, this was more expensive with a price tag of \$305 and it has bulky dimensions of 1.38 x 2.36 x 0.59 in. It was also not known whether this device would be compatible with the software and other hardware which need to be able to communicate efficiently.



Figure 1.10: YostLabs Bluetooth device (yostlabs.com)

Another commercial device called MetaMotionR (MMR) satisfies the requirements for gait tracking of an Afari user. This device is a wearable device that offers real-time and continuous monitoring of motion and pressure, temperature data, and ambient light (MMR). The motion data is captured with a 9-axis IMU. This device also comes with open source APIs supporting Swift, C++, C#, Java, and Javascript and application software for sensor data acquisition. A picture of the device and its phone application is shown in Figure 1.11.



Figure 1.11: MetaMotionR device and phone application (MMR)

The white rectangular prisms are the MMRs which are encased in rubber so they can be attached to the user and the phone application is shown on the left in Figure 1.11. This device has small dimensions of 27mm × 27mm x 4mm in case, a weight of .2 oz, a sampling rate of 100 Hz and the accuracy of the measured angle is <1° RMS (MMR). Furthermore, it is reasonably

priced at \$89.99 for the base version seemingly setting a standard for the market of accurate and versatile activity tracking devices.

1.5.2 Inertial Measurement Units

Inertial measurement units measure linear and angular motion and are capable computing angle of inclination and compass heading (Euler angles). They record data from three different sensors, a magnetometer records the magnetic field strength, an accelerometer records the acceleration, and a gyroscope records the angular velocity. Examples of two different low-cost inertial measurement units are shown in Figure 1.12.

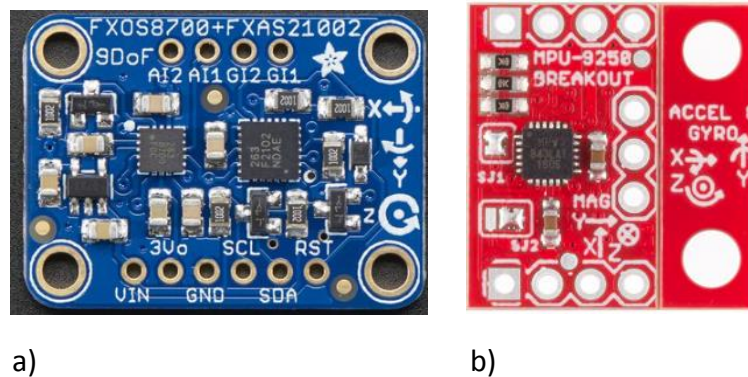


Figure 1.12: Adafruit FXOS8700 Breakout IMU on the left (a) Sparkfun IMU Breakout MPU-9250 on the right (b) (adafruit.com) (sparkfun.com)

The Sparkfun IMU based on the MPU-9250 chip is an I²c device, that allows multiple slave digital integrated circuits to communicate with one or more master chips (sparkfun.com). The Adafruit FXOS8700 IMU, another I²c device, outputs raw signal data that needs processing for it to be useful.

Another advanced, low cost IMU considered was the Adafruit IMU called BNO055 Breakout sensor, shown in Figure 1.13. This IMU has a processor with a sensor fusion algorithm built in to

combine all the data from the magnetometer, accelerometer, and gyroscope and output data you can use in quaternions, Euler angles or vectors.

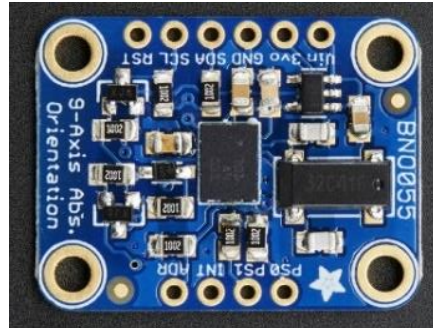


Figure 1.13: Adafruit BNO055 Breakout IMU sensor (adafruit.com)

The specifications for each IMU are in Table 1.1. The voltage range of each device is compatible with most microcontrollers and can be readily powered by a standard LiPo battery. The size and output data resolution between all the sensors had minimal differences so it was not a significant factor.

Table 1.1-Summary of the IMUs Considered for Use

	Supply Voltage	Output Data Resolution	Acceleration full scale range	Size
BNO055 IMU	2.4-3.6V	14-16 bit	$\pm 16g$	20.0mm x 27.0mm x 4.0mm
MPU-9250 IMU	2.4-3.6V	16 bit	$\pm 16g$	20.0mm x 20.00mm x 3.0mm
FXOS8700 IMU	2-3.6V	14-16 bit	$\pm 8g$	28.3mm x 20.5 mm x 3.0mm

1.5.3 Force Measurement Devices

Two common and accurate sensors for force and weight measurements are force sensitive resistors (FSRs) and load cells. Load cells return a signal proportional to the mechanical force applied to the system and this can be done by either pneumatics, hydraulics, or most commonly strain gauges which is shown in Figure 1.14.

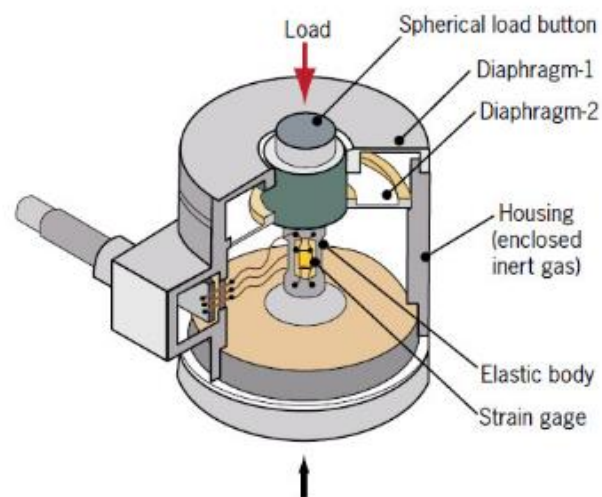


Figure 1.14: Typical load cell based on strain gauge (TekScan).

Load cells that are based on a strain gauge usually implement a Wheatstone bridge configuration shown in Figure 1.15.

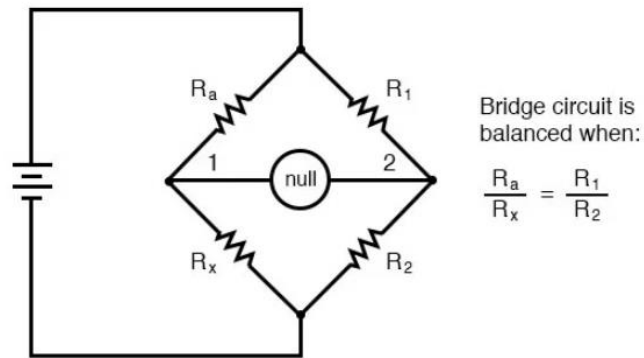


Figure 1.15: Diagram of Wheatstone bridge where R is the resistance (Strain Gauges).

The strain induced on the Wheatstone bridge will change the resistance which can be converted to the force applied with the appropriate calibration factor. Load cells have high accuracy with a <0.1% of full scale and they are robust with minimal hysteresis. However, their bulkiness and rigid construction can be problematic for systems that have limited space.

Force sensitive resistors, sensor shown in Figure 1.16, differ from load cells in that they measure a compressive force directly.



Figure 1.16: TekScan force sensitive resistor.

The force applied to the FSR compresses two layers of a flexible, printed, piezoresistive ink together and this compression results in a proportional change in electrical signal, which can be

calibrated to force (TekScan). FSRs present a few advantages over load cells in that they can be much smaller and lightweight, the sensor shown in Figure 1.16 has a smaller diameter than a dime and a thickness of .2mm. Furthermore, they don't require expensive signal conditioning electronics. However, they have lesser accuracy of around $\pm 5\%$ full scale, sometimes exhibit hysteresis and they need to be calibrated by the user.

1.6 IMU Post Processing Algorithms

Three common algorithms for IMU-based gait measurement are the abstraction model, gait model and direct integration (Zhu et al, 2012). The abstraction model uses neural networks and machine learning methods to estimate the walking patterns. Algorithms using gait models make use of the derived kinematic information from predefined models. Algorithms based on direct integration measure walking acceleration through inertial sensors, so that the velocity and stride length can be derived by single and double integration of acceleration (Zhu et al, 2012). For direct integration to be viable the drift in the sensors needs to be minimized or filtered so it does not accumulate and give inaccurate results.

1.7 Desired Gait Measurements

An IMU can be used to monitor gait and accordingly it is important to understand the gait cycle. A typical gait cycle, as depicted in Figure 1.17, shows the gait characteristics of the right leg for a single stride (Sijobert, Benot, et al, 2015). On the far left of Figure 1.17 a heel strike, the initial contact between the foot and the ground, starts the stance phase. The foot rotates until the zero point occurs in which the foot is parallel with the floor and then rotates further until the toe-off instance occurs which completes the stance phase. After the toe-off instance the leg will leave contact with the ground starting the swing phase while the other leg is in the stance

phase and the swing phase ends when the heel contacts the floor again restarting the cycle with the heel strike instance.

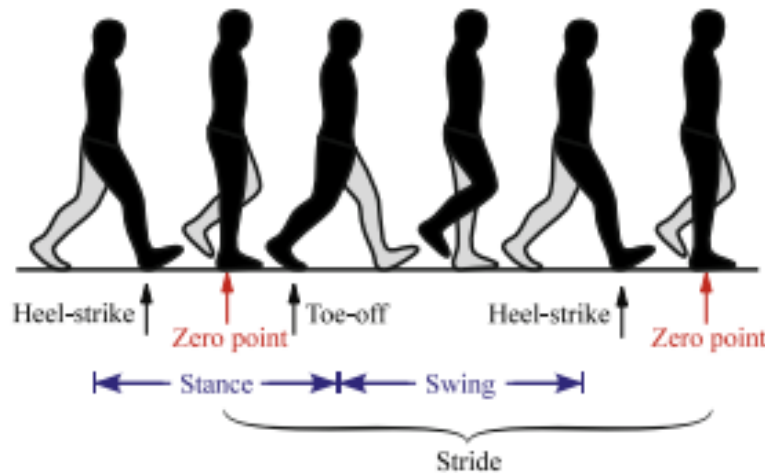


Figure 1.17: Normal gait cycle with characteristic points of the right foot (Sijobert, et al, 2015).

Different gait characteristics which are worthy of analyzing include stride length, swing time, stance time, swing to stance ratio, cadence, heel strike and toe-off angle. The stride length is the distance between successive points in each foot while in contact with the floor, also called zero points as shown in Figure 1.17. The successive points can also be heel strike or the toe off instance to calculate the same stride length. Swing time is the duration the leg is in the swing phase and stance time is the duration the leg is in the stance phase or in contact with the ground. Swing to stance ratio is the ratio between swing time to stance time. Cadence is the number of steps in a minute. Heel strike and toe-off angles are the angles the foot makes with the floor at these instances. Heel strike will be a positive angle whereas the toe-off angle will be negative when measuring the angle counterclockwise from the floor.

Decline in gait speed can be a predictor of future falls so monitoring cadence is valuable.

Besides being a potential warning, it can also be an indicator of physical activity improvement with increasing cadence while using a mobility device. However, cadence increasing too fast could also result in falls so gradual progression is desired. Furthermore, slow gait can be related to affective disorders like depression and bipolar, so these could be detected from the monitoring of cadence (Weiss, 2014).

The heel strike is important because it begins the gait cycle and the orientation of the foot at initial contact can dictate the gait stability for the rest of the stride. "Heel strike with the foot at a 25-degree angle to the floor is the normal occurrence" (Perry, 2002). Following the heel strike there is a motion called the heel rocker which "corresponds to the progression of the limb following heel strike, with the heel serving as the pivot of support and rotation" (Vette 2018). Gait stability during the stance phase will be lost if there is not an adequate heel strike and complete heel strike with toe-descent to foot-flat due to insufficient knee extension or limited range of motion in dorsiflexion (Vette, 2018). Therefore, it can be beneficial to detect toe-walking or early heel rise which can compromise a person's gait stability and increase their chances of falling or cause additional stress in lower body joints.

The angle the foot makes for toe-off can also be important as a study has shown "osteoarthritic knees that progressed had less toeing-out than knees without progression. Greater toe-out was associated with a lower likelihood of progression" (Chang, 2007). A study of four subjects correlating their toe-out angle to their knee abduction moment was performed and the results are shown in Figure 1.18.

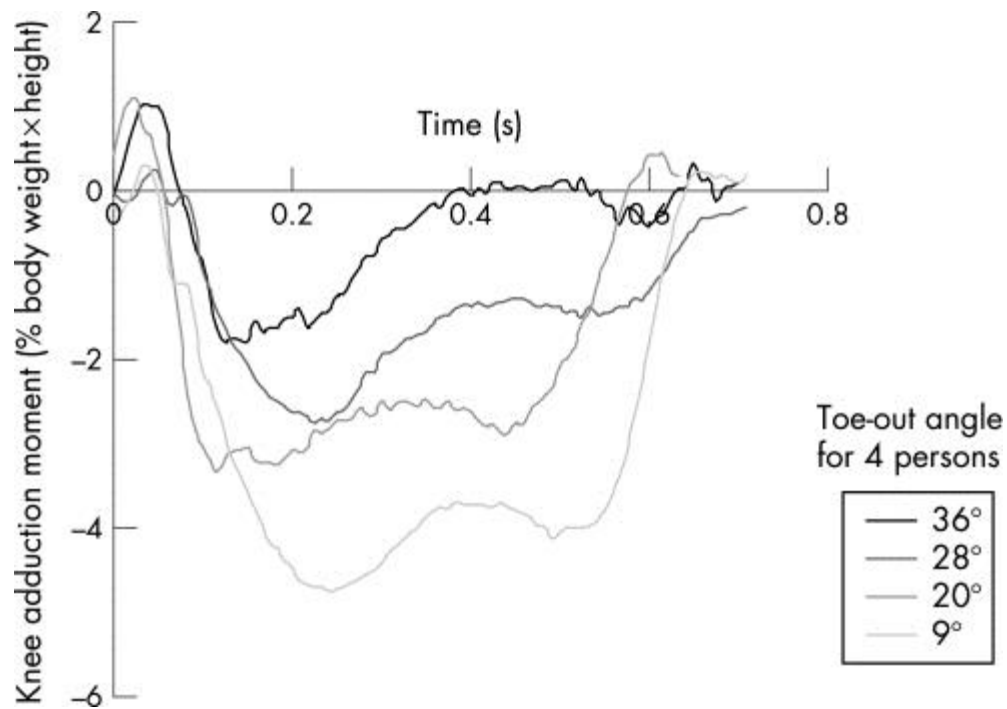


Figure 1.18: Trajectories of the knee adduction moment (N*m) are shown for four participants with different toe-out angles shown on lower right (Chang, 2007).

A greater knee adduction moment will cause more strain in the knees and is more likely to worsen the condition of osteoarthritic knees. Therefore, it could be beneficial for an Afari user that has osteoarthritic knees to monitor the toe-off angle and adjust it to minimize the knee adduction moment lessening the strain. This angle can be detected with the IMU attached to the ankle which records the tilt angle of the foot in the sagittal plane. This will be the minimum angle for each stride and the average toe-off angle can be computed from a subject's walking or running session.

1.8 Project Objectives and Scope

The purpose of this study is to evaluate and improve the monitoring system called INTRAC™ that is intended for Afari assistive device. This monitoring system can be used as a cost-effective balance activity tracking and measuring system. It includes an IMU attachment so that stride, balance, and gait can be assessed if desired. INTRAC™ measurements of the subject's usage include load bearing weight and its distribution, stride length, stride regularity, cadence, distance travelled, average speed, and swing to stance ratio, and heel strike and toe-off angles.

Chapter 2 will give an overview of the Afari activity tracking system and describe the sensors that were tested including their design and calibration. Chapter 3 describes the uses of each component of the activity tracking system and the data retrieved from each. Chapter 3 also shows how the components work as a system and the steps needed to use the system with the INTRAC software. Chapter 4 gives a summary and recommendations for the development of the Afari activity tracking system.

CHAPTER 2

INTRAC MONITORING SYSTEM FOR AFARI

2.1 Overview of the INTRAC System

INTRAC™ is a wireless sensing system based upon Bluetooth Low Energy (BLE) technology developed at the University of Maine for Afari. It is integrated with an IOS or ANDROID smartphone application. The software also works on the MSWindows or OSX based environments that can access Bluetooth 4.1 or later. It uses a master/slave design, as shown in Figure 2.1, where a single BLE unit communicates data from a slave unit to the smart device hosting the application. Each of the modules can work either individually or in tandem with the other modules. The system currently includes the modules listed in Table 2.1 items 1-4.

Table 2.1 – Current Features of INTRAC

Feature
1. Left and right weight bearing and balance indicator.
2. Speed and distance sensing.
3. Ankle or shoe mounted inertial measuring unit (IMU).
4. Smartphone application.

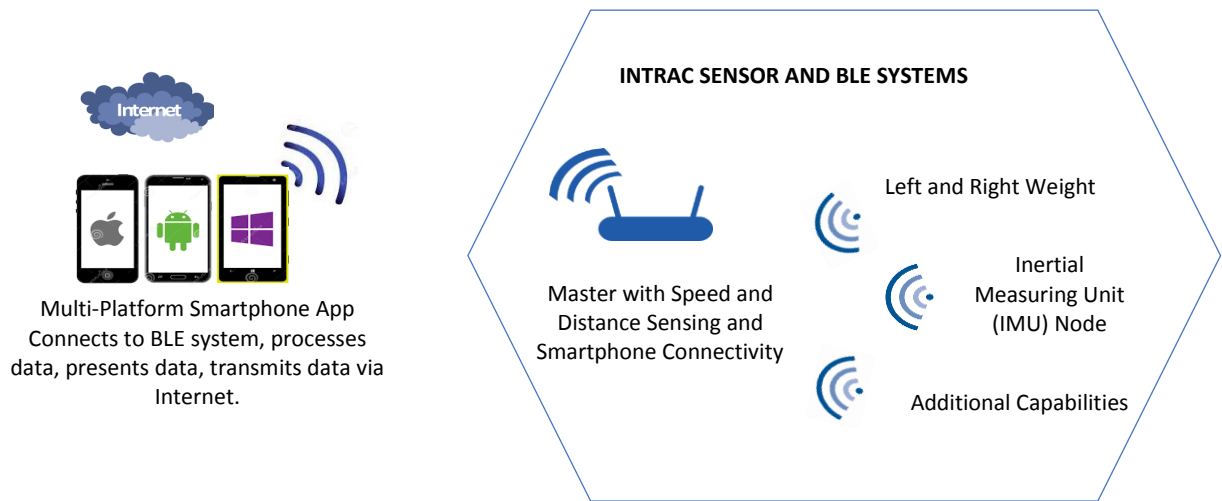


Figure 2.1: INTRAC System Design Overview

2.1.1 Weight Measurement Module - Weight bearing and balance indicators were designed and created at UMaine and are strain gauge based load sensing devices. The original design employed an instrumented handlebar with the electronics mounted beneath the Afari arm pad. Some difficulties found with this design included protection of the sensors by creating a pocket into the handle bar material caused a structural failure and difficulty with cabling going through the bar. An improved design was achieved as a result of the current efforts by integration shear force sensing units directly into the Afari arm rest pads. Details of this design is described in Section 2.3. In the standalone mode the left sensor acts as a master and transmits both sets of data to the smartphone. The sensors can also both be put in the slave mode and transmit their data to the speed/distance module that always acts as a master unit when it is present.

2.1.2 Speed/Distance Measurement Module – The speed distance measurement system uses a set of magnets and a magnetically actuated reed switch to estimate distance travelled. Details of the design are described in Section 2.4. Testing was performed to establish the precision achieved when using an increasing number of magnets, which is end user selectable in the smartphone application. As part this effort, mounts were designed and fabricated for attaching the magnets to the spokes of the Afari. A housing was created for the wireless unit which is always placed in the role of the master and communicates with the smartphone. Due to the limited amount of space a small profile unit was fabricated onto a PC board and the unit housed the BLE wireless, battery, charging circuit, and reed switch. The reed switch is mounted in an extension so that it lines up across from the plane of the magnets. Electrical contact is temporarily made as a magnet passes by the switch. The contact is sensed by the BLE unit similar as done in bicycle speed and distance sensors.

2.1.3 Ankle or Shoe Mounted Inertial Measuring Units - It is desirable in some instances to track a person's gait and angle of inclination. That task can readily be accomplished using an IMU as described in Section 1.5.2. The Bosch BNO055 unit was selected for our purposes and was integrated into 2 devices, a clip-on shoe mounted version and an ankle strap version shown in Figure 2.2. Both versions use identical hardware that includes the wireless unit, IMU, battery and charging circuit. The clip-on IMU may move slightly more than the ankle strapped IMU which could compromise the accuracy of the gait feedback. However, a subject may have difficulty strapping the IMU around their leg or may not like the IMU around their leg so a clip-on IMU was also designed to attach to the subject's shoe.



Figure 2.2: Ankle strapped IMU is on the left and the clip-on IMU is on the right.

2.1.4 Foot Pressure Measurement Unit - The foot pressure measurement unit is latest module to be developed and is currently still in the proof of concept stage as shown in Figure 2.3. It uses a force sensing resistor or capacitive force sensor embedded into a shoe insole. Figure 2.3 shows the mold used on the left and the first attempt at casting this device. Ultimately the force sensing resistors used in this device will be attached to the wireless system. This mold attached with force sensors would be inserted into an Afari user's shoes similar to a gel insole while being comfortable and not affecting their walking behavior. The purpose of the foot pressure measurement unit is to get more information of an Afari user's weight distribution while walking or running. This additional information could give the user more insight on their balance for their lower body whereas the load cells give information for their upper body balance during exercise and together the total force distribution can be determined. The testing of the accuracy and repeatability of four different force sensors will be described in Section 3.3.



Figure 2.3: Foot sensor mold and prototype.

2.2 Electronics and Software

BLE modules were based upon the Cypress programmable system on a chip (PSOC) technology that integrates microprocessor capabilities with analog and digital I/O, multiplexing, I²C and Bluetooth 4.1+ capabilities. The modules were programmed in C to perform their desired functions. In this environment the PSOC is set in a client or peripheral mode or combinations thereof to perform their desired function. The module allows direct connection or can be programmed to continually transmit data.

The smartphone application was programmed in Radstudio™ using C++. This is a multi-device platform where the same code with some minor modifications can be used for the Android, IOS, MSWindows or OSX environments. The alpha version of the programming is completed and some aspects are still under development. To date, the Apple development mode is being

used for IOS and OSX. This requires an Apple developer account and allows the development version to be download only to specific devices that are attached to the system. Eventually, the program would need to be deployed using the Apple Appstore protocols. On Android and MSWindows the program can currently be loaded in an executable form to operate on these devices.

In the long term, plans are to integrate the INTRAC software system with other tracking devices such as Fitbit for vital signs and additional activity tracking. This data set is of great significance to our target population, elder mobility impaired users and their providers. Real-time, comprehensive gait monitoring during regular daily activity, with added vital signs data, formatted on easy to read interfaces for both providers and users can immediately, precisely, and non-invasively identify health improvements and, on the flip-side, risks for decline.

2.3 Arm Rest Load Cell Design

A load cell monitoring system was implemented on the Afari to measure the weight applied to each arm rest. The load cells are comprised of strain gauges configured in a full Wheatstone bridge circuit and can be calibrated in terms of voltage output for a given amount of force.

Once calibrated, the force applied to each arm rest can be obtained from the voltages acquired through the INTRAC sensing system. The internal components of the load cell can be seen in Figure 2.4. The circuit board on the left contains a programmable system on a chip (PSOC) incorporating the Bluetooth radio, load signal conditioning, charging circuitry and battery. The PSOC in a Cypress BLE module that has A/D, I²C and SPI capability. The load cell amplifier is used to condition, amplify and acquire the strain gage signals and is based on the HTX 711 IC. It is

responsible for the A/D conversion in a 24-bit format and passes the data to the PSOC using SPI at a selectable rate of 8 or 80 samples per second. The load cell structure contains an aluminum part shown on the right and contains two pairs of shear type strain gauges. It was designed to bolt directly to the Afari arm rest. It is interfaced to a Cypress CY8CKIT-042-BLE module, load cell amplifier and LiPo charging circuit shown in Figure 2.4. The module is powered using a LiPo rechargeable battery that outputs 3.7V and has a capacity of 600 mAh.

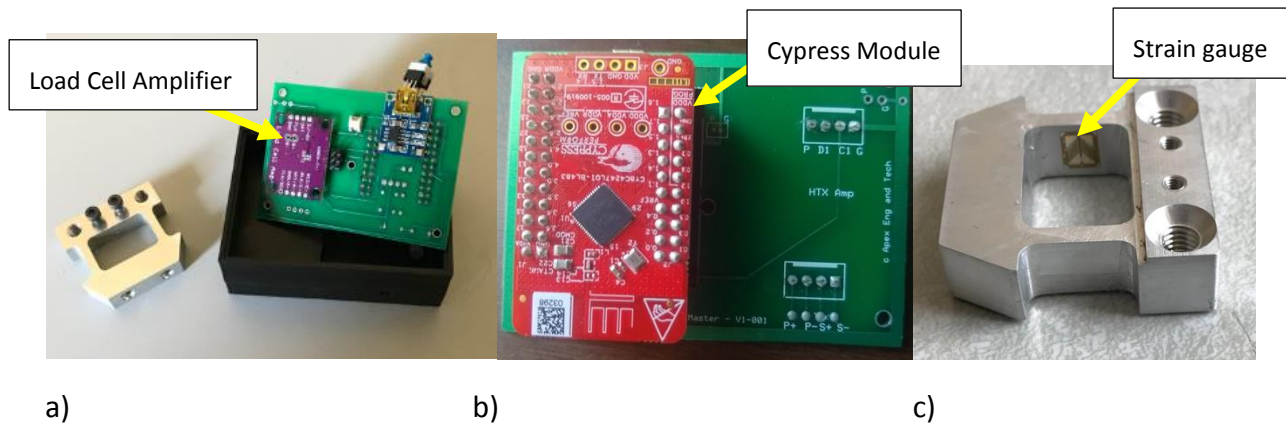


Figure 2.4: a) Load cell monitoring system with all components b) other side of breadboard c) aluminum interface with strain gauge attached.

The components fit inside a PLA housing that is bolted under the arm rest as shown in Figure 2.5. The housing design includes an on/off switch, charging port and led indicator. It was created in SolidWorks and 3D printed using PLA material.

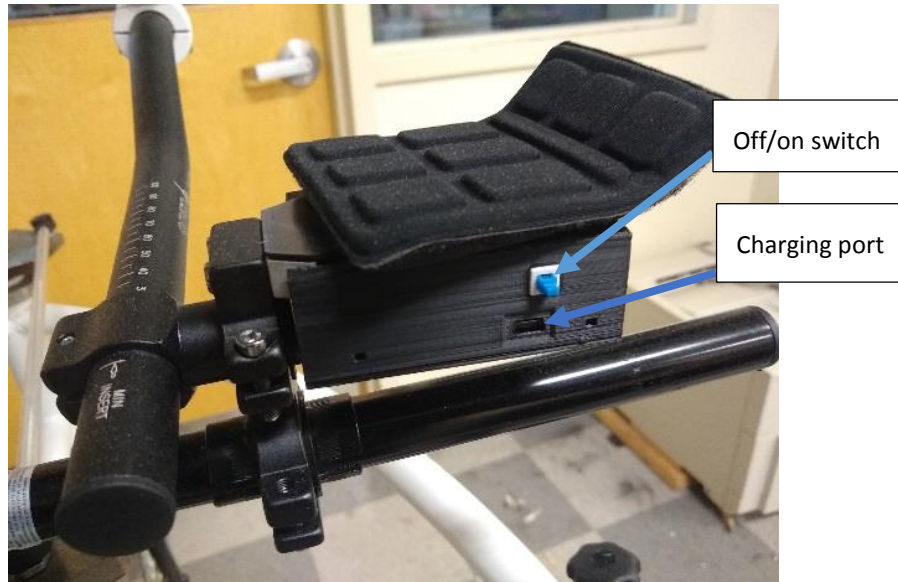


Figure 2.5: Weight monitoring system's placement on the Afari.

2.3.1 Load Cell Calibration:

Load cell calibration was performed to convert the digitized value of the analog input voltage, induced by force on the load cell, to an accurate reading of the user's weight transferred through their forearms. The calibration setup is shown in Figure 2.6 and includes a custom-made hangar that applies force to the armrest and calibrated weights in 5.0 pound increments are suspended from the hangar. More weights can be stacked on the five-pound weight shown in Figure 2.6 and the total available load is 50 pounds.



Figure 2.6: Calibration setup for the Afari weight bearing monitoring system.

Ten calibration runs were performed and the standard deviation between calibration factors is calculated to ensure accuracy and repeatability. The procedure to perform the calibration is as follows:

1. Turn on each load cell by pressing the blue on/off buttons, a green light should appear.
2. Start the INTRAC program and connect to the load cell, the light should turn white and then blue when Bluetooth communication is established.
3. Set the calibration factors to 1.0 and tare the weight reading with no weight applied to the Afari as shown in Figure 2.7. The tare takes the average of 8 readings.

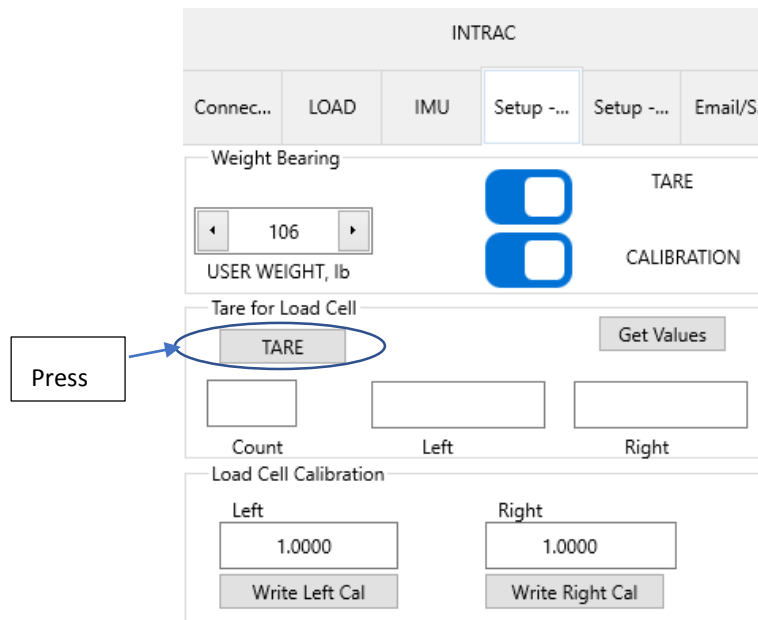


Figure 2.7: Load cell calibration user interface.

4. Place calibration rig on left load cell as shown in Figure 2.7 and tare to get the reading for 1.044 kg, the weight of the calibration rig.
5. Attach weights to rod in increments of 5 pounds until 50 pounds is reached and record each reading for the corresponding weight.
6. Perform a linear regression analysis using software such as MS Excel to determine the calibration constant. It is expected that this should give a calibration curve with $R^2 > 98\%$.
7. Repeat steps 4-6 for the right load cell as well.
8. Perform the previous steps for the position of the calibration rig on the inner and outer part of the load cell to observe the dependence of weight on the position.

In addition, the previous steps were performed for the load cell at decreasing voltages until the battery turned off to assess the influence of the battery voltage on the calibration constant, if any.

2.3.2 Load Cell Calibration Results:

After 5 calibrations were performed for the left and right load cell, the data was analyzed as presented in Figures 2.8 and 2.9, respectively. The average R^2 value for the linear regression for the left load cell data was a 99.95% and the average calibration constant was .03376 pounds/AD count with a deviation of $1.3\text{E-}4$ or 0.40%. For the right load cell, the average R^2 value for the linear regression of the data was a 99.96% and the average calibration constant was -0.02655 pounds/AD count with a deviation of $9.27\text{E-}4$ or 3.49%.

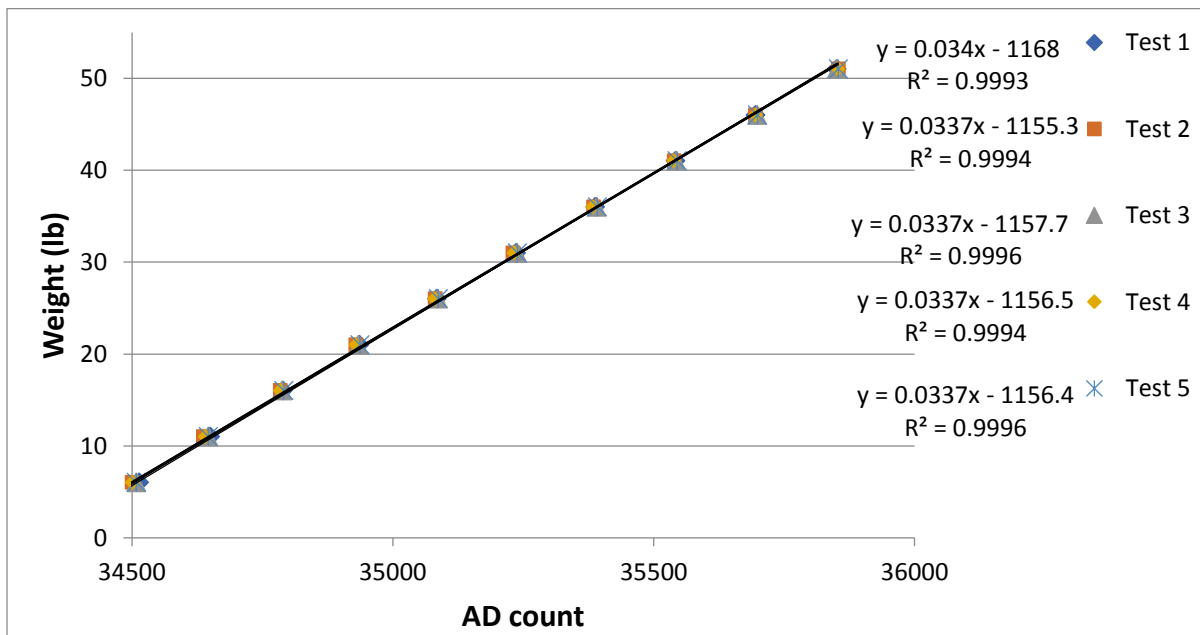


Figure 2.8: Weight (lb) with respect to AD count for left load cell calibrations.

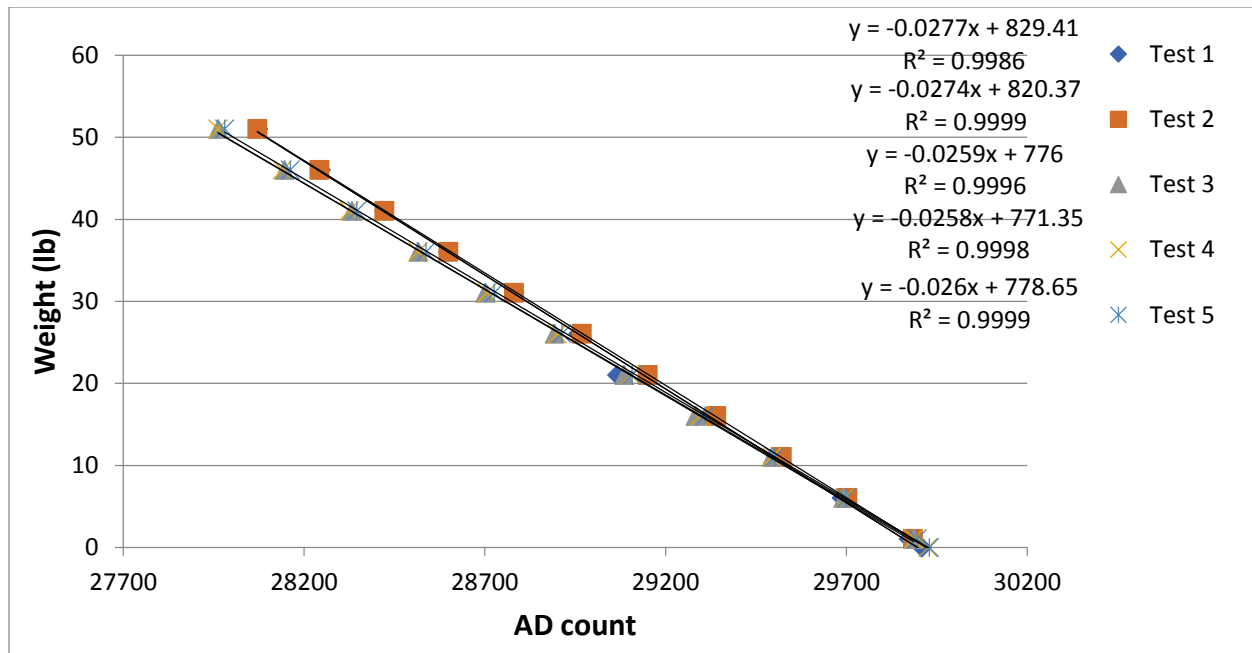


Figure 2.9: Weight (lb) with respect to AD count for right load cell calibrations.

2.3.3 Dependence on Position of Weight:

Acknowledging a person would likely move their forearm along the arm rest, testing was done to assess the influence of position on the weight readings. Figure 2.10 shows the calibration positions, outer part, middle part, and inner part of the arm rest, that were tested.



Figure 2.10: Weight dependence positions.

Two calibrations were performed for each position, inner, middle, and outer, and the AD count was recorded for each applied weight. The left load cell had a calibration constant average of 0.03245 pounds/AD count for weight on the inner side, 0.0346 pounds/AD count for the middle position, and 0.03405 for the outer side. The difference between the outer and inner calibration constant is 0.0016 pounds/AD count or 4.8%. This indicates that the position of the center of force has an acceptable influence on the weight reading.

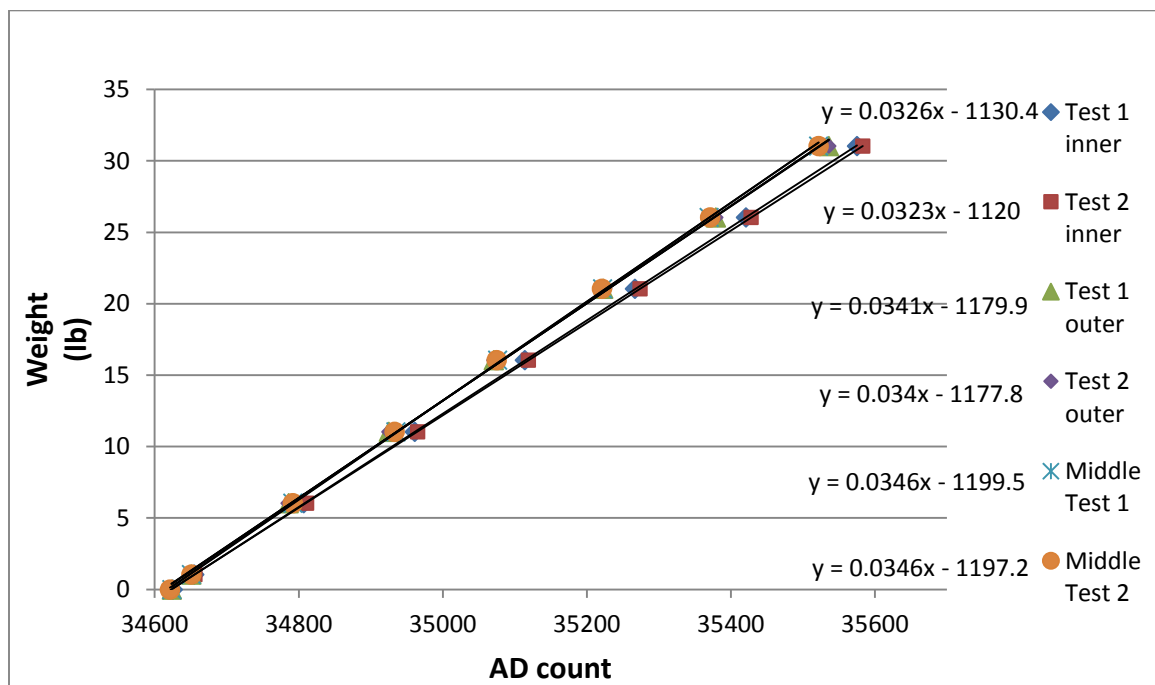


Figure 2.11: Weight (lb) with respect to the AD count for the left load cell.

2.3.4 Dependence on Battery Life:

The expected life of the battery was assessed by leaving it on and recording the voltage with a multimeter in intervals and recording the time. The voltage of the load cell battery decreases at a steady rate until it reaches 3.5 V after 11 hours then it drops quickly until it is off after 12 hours shown in Figure 2.12.

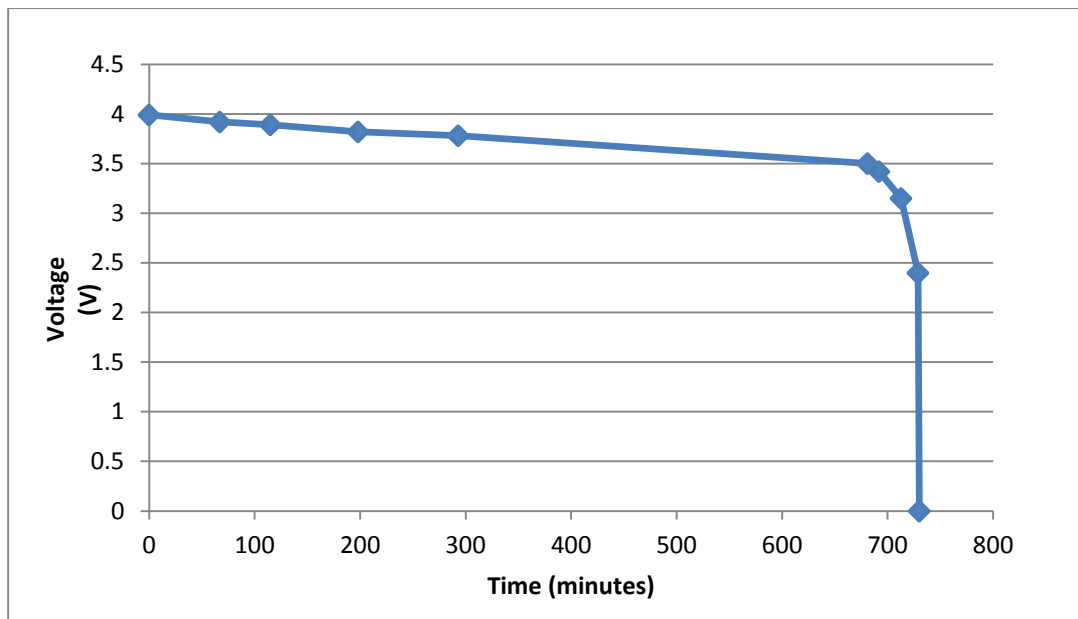


Figure 2.12: Load cell battery's voltage (V) with respect to time (minutes).

The battery voltage has a negligible effect on the calibration constant as it only varies at most by 3.1% as shown in Figure 2.13. A calibration was performed for a voltage of 3.97 V, 3.5V, 3.1 V, and approximately 2.5 V. The last voltage has a range of 2.6 V to 2.4 V because it drops quickly when it is that low and a calibration takes a few minutes as weights need to be added and the AD count needs to be recorded for each weight. Therefore, the load cell will perform effectively until the battery turns off.

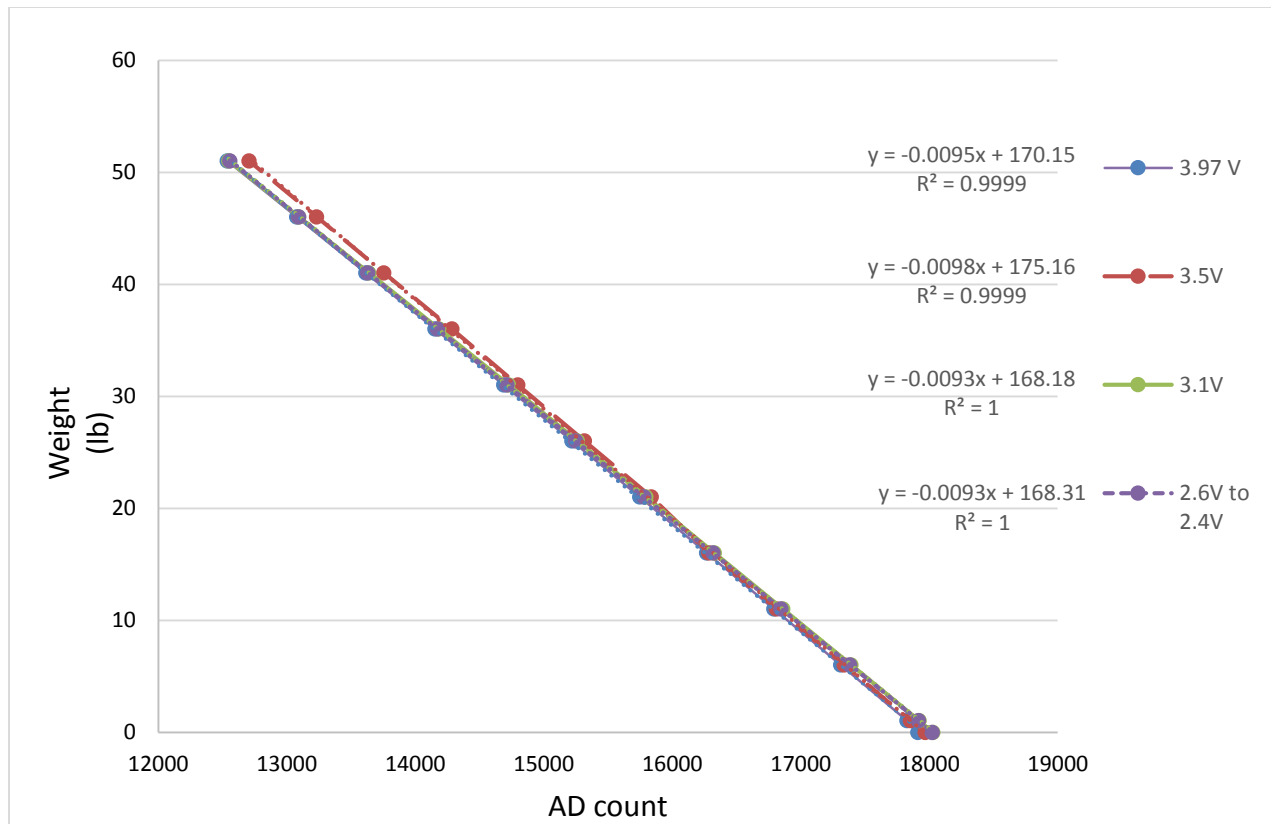


Figure 2.13: Weight (lb) with respect to AD count of different battery voltages.

2.4 Inertial Measurement Unit Design

An inertial measurement unit was used in the INTRAC system to measure the tilt angle of a user's foot. Proof of concept models of the ankle and shoe clip versions were described in Section 2.1.3. Although the embedded urethane models are thought to be a good waterproof option for outdoor use, changes to the prototype design were not possible. Accordingly, a model was created in a 3D printed housing to readily allow changes in the components, if desired. Figure 2.14 shows the internal components of the small wireless device that is attached to the user's shoe around their ankle with a clip. Figure 2.15 shows the IMU case with clip attached.

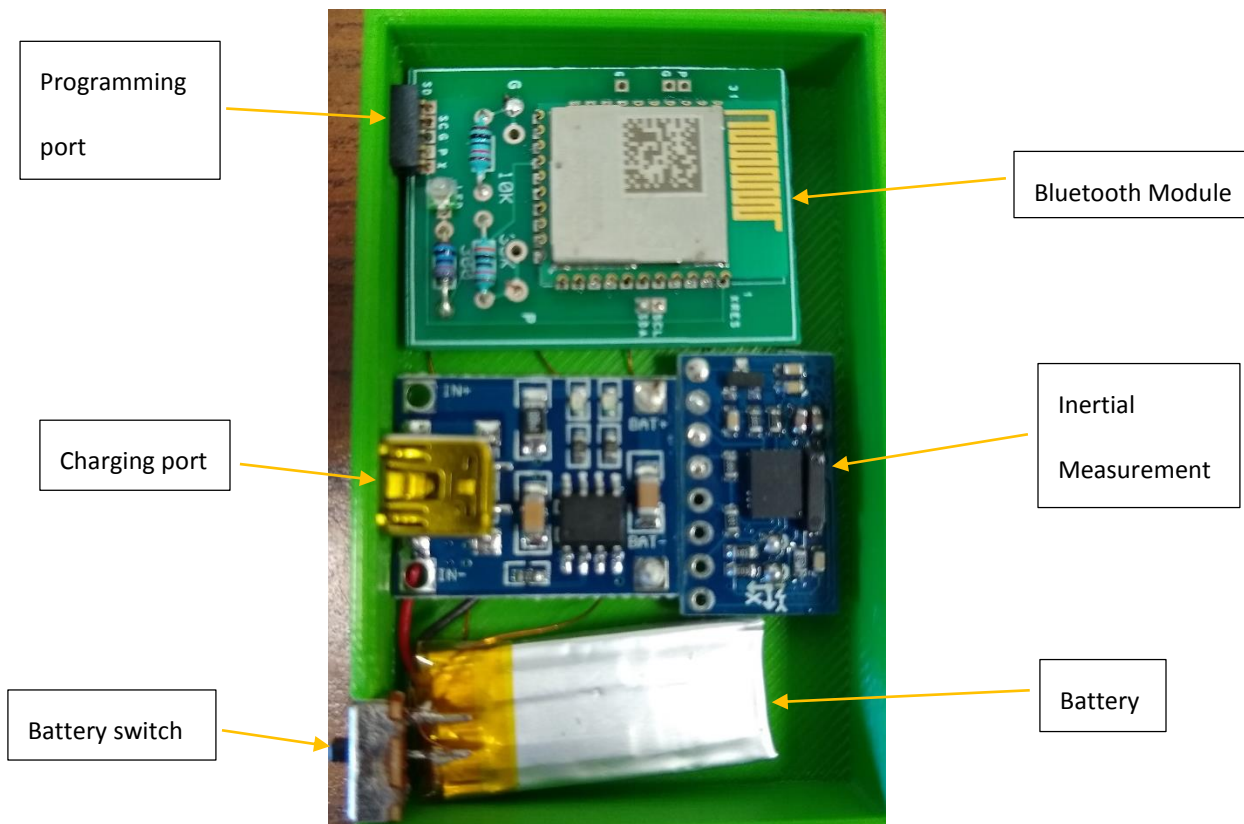


Figure 2.14: Wiring and components of the inertial measurement unit device.

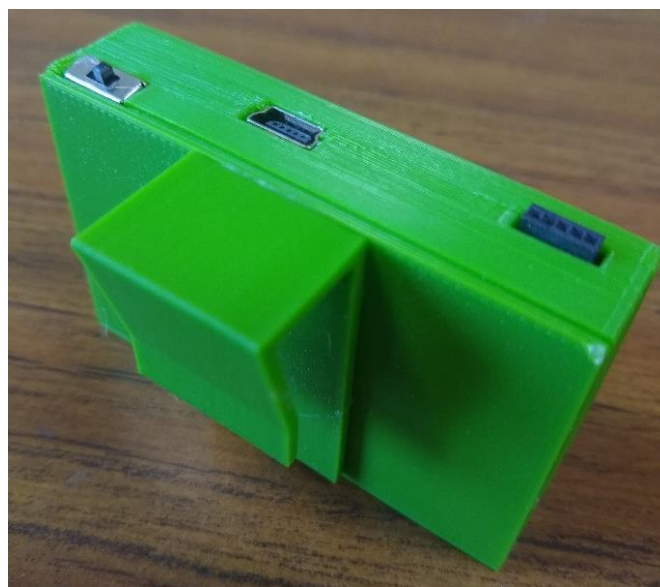


Figure 2.15: IMU case with clip attached.

The sensor fusion algorithm of BNO055 IMU sensor combines the accelerometer, magnetometer and gyroscope data into stable three-axis orientation output. The manual (Bosch SensorTec, 2016, p. 22) describes how this sensor fusion algorithm works in more detail:

“Sensor fusion modes are meant to calculate measures describing the orientation of the device in space. It can be distinguished between non-absolute or relative orientation and absolute orientation. Absolute orientation means orientation of the sensor with respect to the earth and its magnetic field. In other words, absolute orientation sensor fusion modes calculate the direction of the magnetic north pole.”

Furthermore, the manual describes the different modes it can operate under:

“In non-absolute or relative orientation modes, the heading of the sensor can vary depending on how the sensor is placed initially. All fusion modes provide the heading of the sensor as quaternion data or in Euler angles (roll, pitch and yaw angle). The acceleration sensor is both exposed to the gravity force and to accelerations applied to the sensor due to movement. In fusion modes it is possible to separate the two acceleration sources, and thus the sensor fusion data provides separately linear acceleration (i.e. acceleration that is applied due to movement) and the gravity vector” (Bosch SensorTec, 2016, p. 22). In the sensor fusion mode the maximum throughput of the BNO055 is 200 samples per second.

2.4.1 Inertial Measurement Unit Calibration

The BNO055 IMU’s calibration is important because the magnetometer needs to be aligned with the Earth’s magnetic pole so the sensor is in the correct orientation frame. The BNO055 IMU doesn't contain static memory to store the calibration constants. Therefore, a new

calibration would need to be performed every time the device starts up. However, since the change in calibration factors is negligible after the initial calibration, they were stored on the static memory of the Cypress PSoC module and automatically uploaded to the BNO055 on startup. Below are the steps for the initial calibration of the BNO055 IMU:

1. To calibrate the gyroscope the IMU must stand still in any position.
2. Normal movement or Figure eight motions will calibrate the magnetometer.
3. To calibrate the accelerometer the IMU should be standing still momentarily on each 6 of its faces.

The Cypress code was written so the LED on the module would turn blue once the calibration was complete and subsequently stored the constants in the static RAM.

2.4.2 Inertial Measurement Unit Verification Test

It is important that the inertial measurement unit records the heel strike at the correct time so the stride length and cadence are accurate. The IMU was used simultaneously with a Vicon motion capture camera system and their heel strike times were compared. A subject placed an IMU and optical markers as shown in Figure 2.16 and walked on a treadmill while both systems were recording.

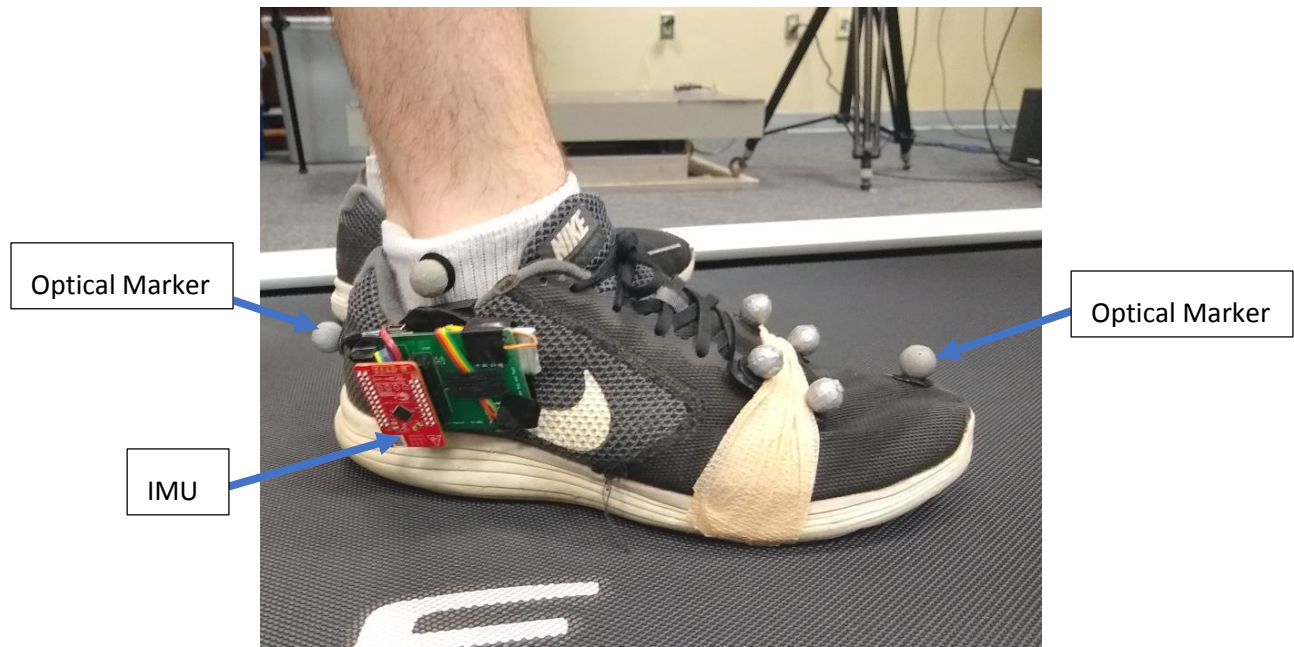


Figure 2.16: Placement of IMU and optical markers.

The IMU measures the foot-to-floor angle and the maximum positive angle corresponds to the heel strike. The Vicon motion capture system was used to measure the anterior (forward) and posterior (backward) movement of the heel marker. The maximum anterior or forward displacement corresponds to the heel strike as the foot will move backwards as soon as it contacts the treadmill. To synchronize the two systems a kick was performed to signal the start of the trial which would be a large peak for both the foot-to-floor angle and forward displacement. Once the timing was synchronized, the foot to floor angle measured by the IMU and displacement measured by the Vicon were graphed shown in Figure 2.17.

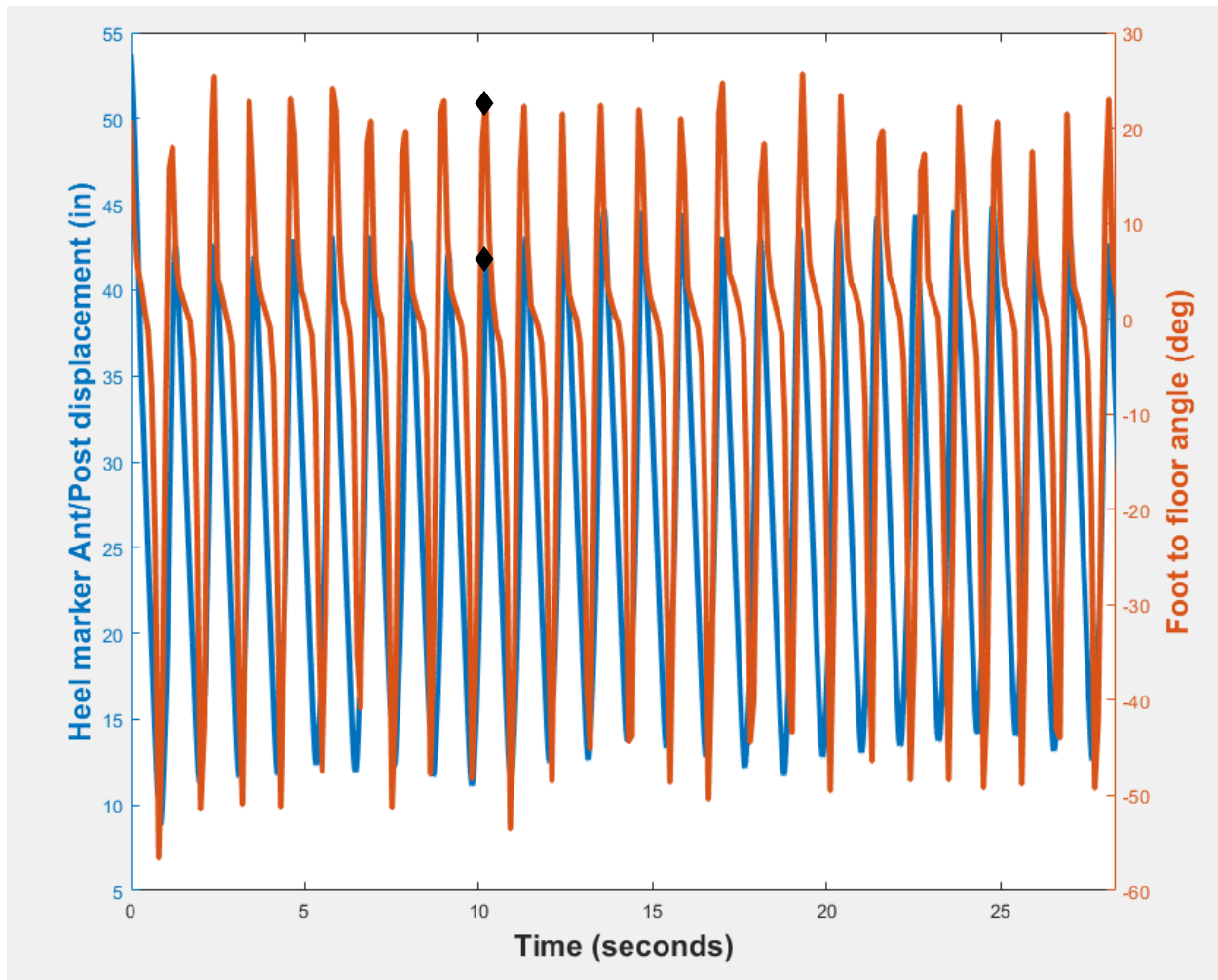


Figure 2.17: Displacement of the heel marker (inches) on the left axis and the foot to floor angle (degrees) on the right axis with respect to time (seconds).

The peaks of the foot to floor angle, orange line, and the heel marker anterior (forward) and posterior (backward) displacement closely align. The peaks are labelled with black diamonds on the eighth cycle to show the time difference. The time difference for this trial was 0.0034 seconds, calculated with MATLAB.

2.5 Speed and Distance Sensor Design

Figure 2.18 shows the speed and distance sensor module. This module is attached to the wheel of the Afari and is the master device for the Bluetooth system so it needs to be turned on, by pressing the blue switch, for the IMU and load cells to transmit data.

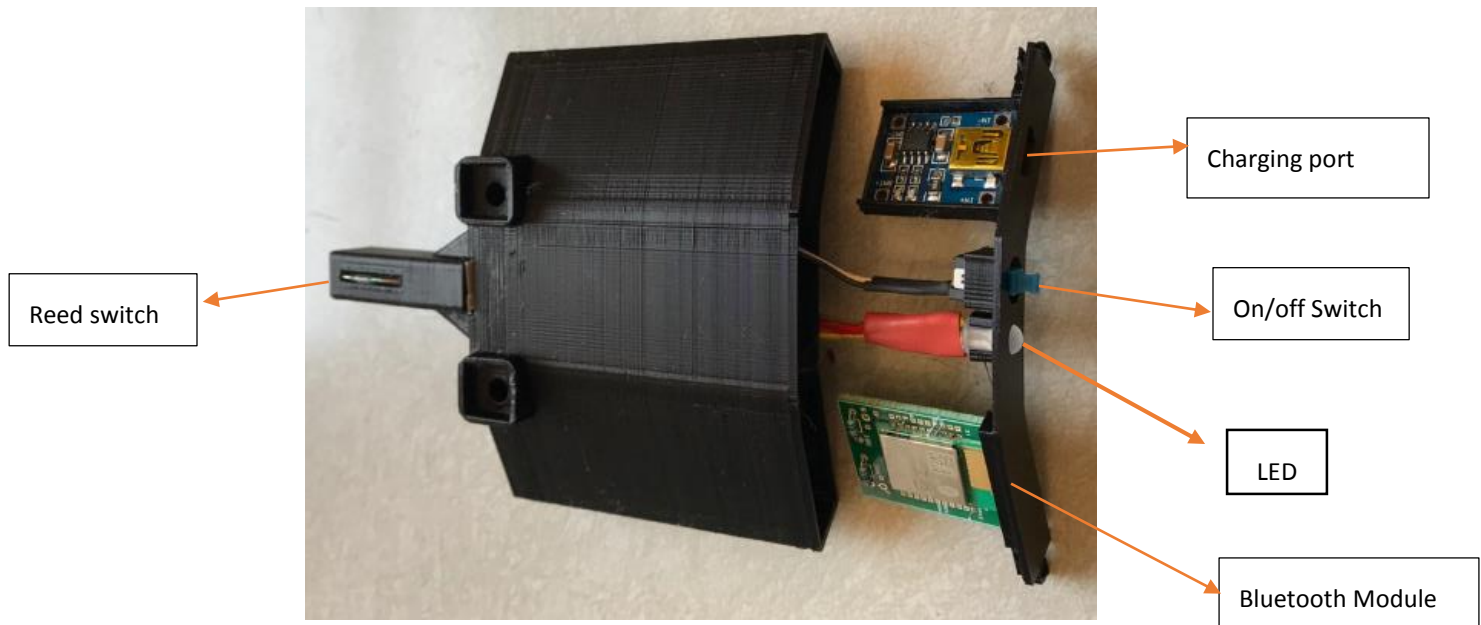


Figure 2.18: Internal components of speed and distance sensor and the 3D printed housing made in PLA.

The reed switch, the sensor used to find the speed and distance, is shown in more detail in Figure 2.19.

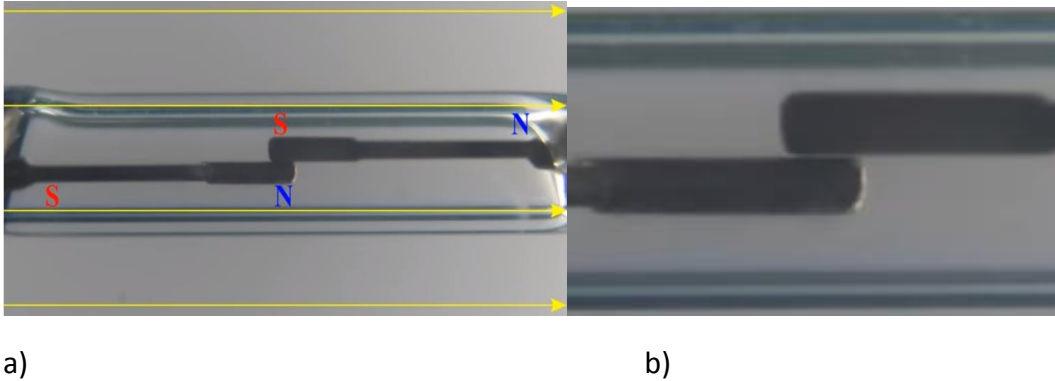


Figure 2.19: a) The Reed switch making contact in presence of magnetic field and b) shows a small gap when there is no magnetic field (Sándor, Zátonyi).

The magnets placed on the spokes of the wheel of the Afari, shown in Figure 2.20, close the gap between the two ferromagnetic flexible metals when they pass close enough to the switch, and a change in voltage is recorded. After passing by the switch opens back up resulting in a voltage pulse. Measuring the diameter of wheel allows the distance traveled to be computed with the circumference distance formula, distance = $\pi \times \text{diameter}$. The diameter of the current Afari wheel is 2.17 feet so a full revolution of the wheel is 6.79 feet in linear distance traveled. Therefore, the distance is measured by dividing the circumference by the number of magnets to find the distance traveled each time a magnet passes the reed switch. The magnets need to be evenly spaced for the distance to be uniform. The resolution of the distance can be improved with more magnets. The time is logged when the reed switch is activated so the speed can also be calculated as change in distance with respect to time.



Figure 2.20: Placement of magnets on wheel on the left and close-up of magnet in 3D printed holder on the right.

2.5.1 Speed and Distance Sensor Calibration

The number of magnets was increased a few times to increase the resolution of the distance travelled so the stride length would be more accurate. Currently there are 18 magnets on the wheel which gives a distance resolution of 0.377 feet. 98.09 feet was measured with a distance measuring wheel and marked and compared with the distance measured with the Afari for 9 and 18 magnets. Their results are shown in Table 2.2.

Table 2.2-Distance Recorded

	Trial 1 (feet)	Trial 2 (feet)	Trial 3 (feet)
9 magnets	97.77	98.43	97.77
18 magnets	97.77	98.09	97.77

These distances are all within 0.33 feet of the distance of 98.09 feet recorded with the distance measuring wheel which is adequate for Afari's purposes.

CHAPTER 3

SYSTEM TESTING

3.1 Testing Conditions and Setting

System testing was performed using a design team member to verify the INTRAC system. The test user of the Afari was a 27-year-old male weighing 180 pounds. The tests were performed in a parking lot on the University of Maine campus, shown in Figure 3.1, on an 85° F day in July of 2019. Three tests were performed in which the user was instructed to apply none of their body weight, 25% of their body weight, and 50% of their body weight to the arm rests for a 30 second duration. Another 180 second test was performed for 50% unweighting of body weight to see the effects of longer Afari use. The user can check the percent body weight that is applied through the phone application shown in Figure 3.27. The speed and distance, foot to floor angle, and the load applied to the arm rests was recorded for each test.

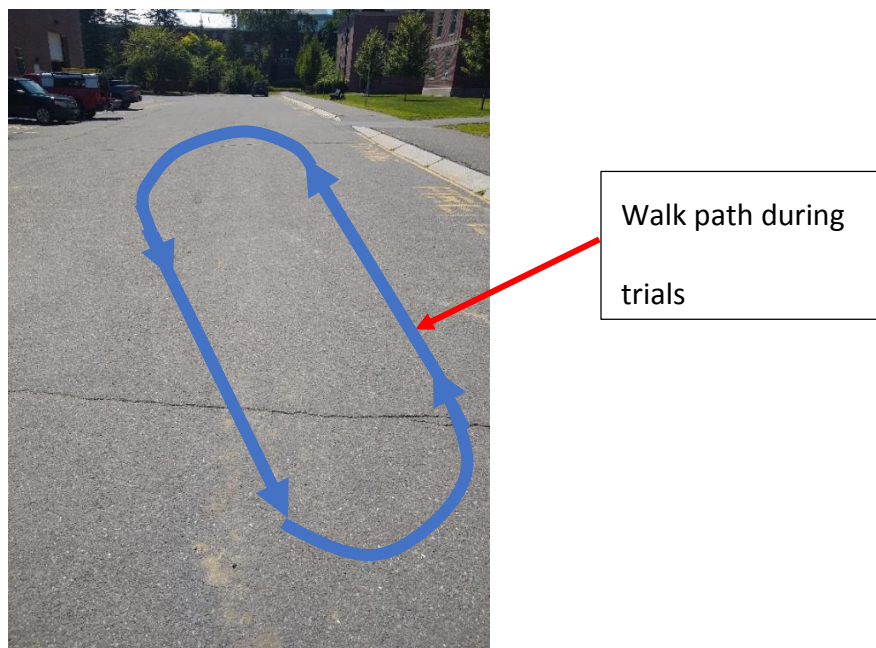


Figure 3.1: Parking lot test setting during Afari use.

3.2 Speed and Distance Sensor Procedure

The speed and distance sensor is the master module for Bluetooth communication so it must be turned on for the other devices to transmit data. The blue switch on the bottom face shown in Figure 2.16 needs to be pressed to turn on the device. This device records the distance travelled when the user presses start on the INTRAC phone application that will be described in Section 3.8.

3.2.1 Speed and Distance Sensor Results

After a data set is taken while using the Afari and e-mailed to the user as a .csv file, it is post-processed in MATLAB. The first step is to load the file into MATLAB and then the data is manipulated to acquire meaningful graphs. The distance vs. time was graphed in MATLAB for each test, shown in Figure 3.2, 3.3, and 3.4. The average speed can be calculated from the distance as the change of distance over time from start to end and this will be shown in Section 3.8. This distance is also used in conjunction with the heel strike times to calculate stride length which will also be described in Section 3.8.

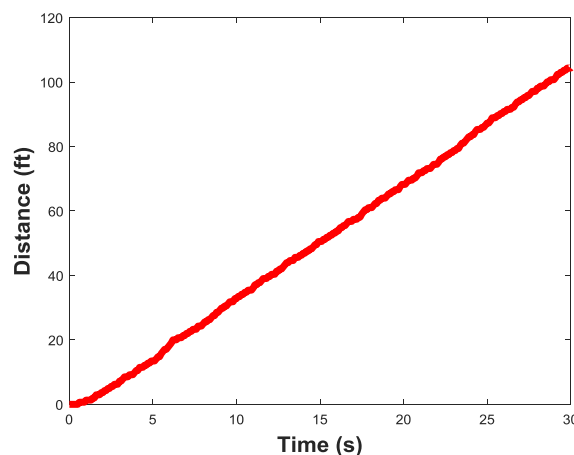


Figure 3.2: Distance (ft) travelled with respect to time (s) for no unweighting.

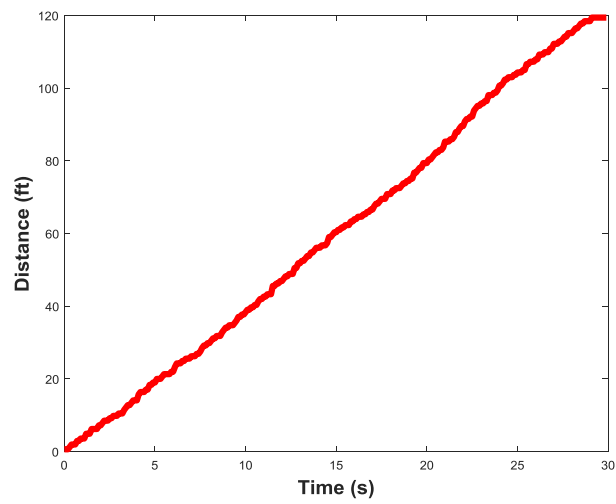


Figure 3.3: Distance (ft) travelled with respect to time (s) for 25% unweighting.

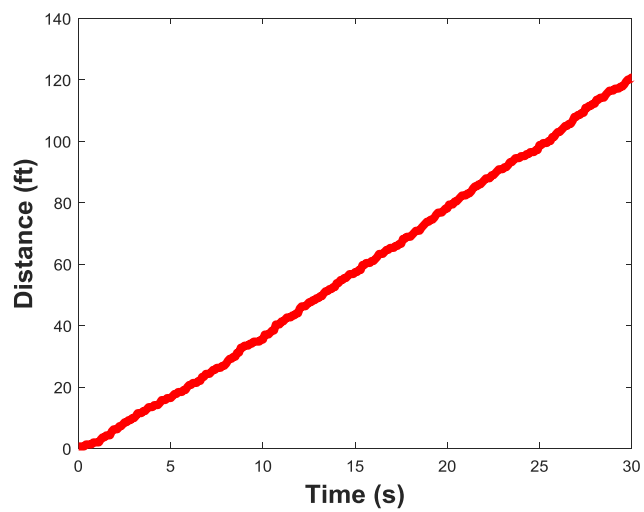


Figure 3.4: Distance (ft) travelled with respect to time (s) for 50% unweighting.

3.3 Load Cell Monitoring System Procedure

As mentioned in Section 3.2, the speed and distance sensor needs to be turned on for the load cells to transmit data when they are configured in the slave mode. To turn on the load cells blue switch shown in Figure 2.4 is pressed for each load cell device. If it is out of battery a type mini-b USB cable needs to be inserted into the charging port shown in Figure 2.4. Once they are both turned on and the LEDs turn blue, they are ready to be connected to the phone application, so data can be retrieved. For the first test the user did not place their forearms on the armrests. For the second test, the user attempted to apply 25% of their body weight, or 45 pounds total, throughout the trial. For the third test the user attempted to apply 50% of their body weight, or 90 pounds total, throughout the trial.

3.3.1 Load Cell Monitoring System Results

The right and left load applied from the user's forearms is graphed for the three tests in MATLAB shown in Figure 3.5, 3.6, and 3.7. As expected, the test with no unweighting showed that no load was recorded by the load cells as shown in Figure 3.5.

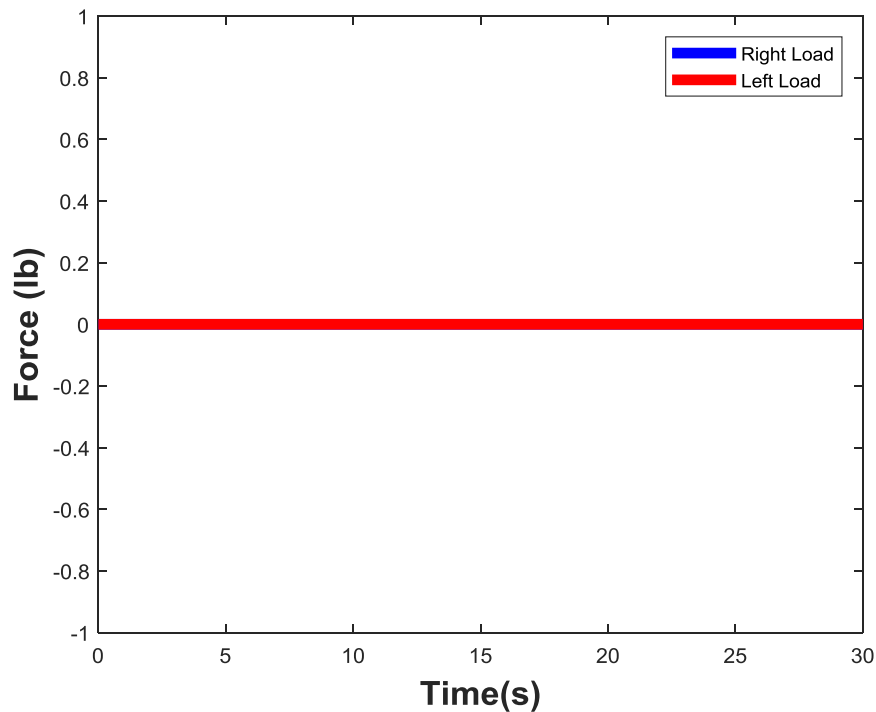


Figure 3.5: Force (lb) applied to arm rests with respect to time (s) the test for no unweighting.

Results of the test with 25% unweighting (45 lb. total) is given in Figure 3.6. The user applied 10 pounds more on the right side than the left side at the start of the test but the loads converge slightly above 25 pounds after 5 seconds. The load application stabilized to some degree during the 5-25 second period. The drop in load at 20 seconds occurred as the user went over a bump on the pavement. The load drop at the end of the 30 second period was due to the user stopping with the device.

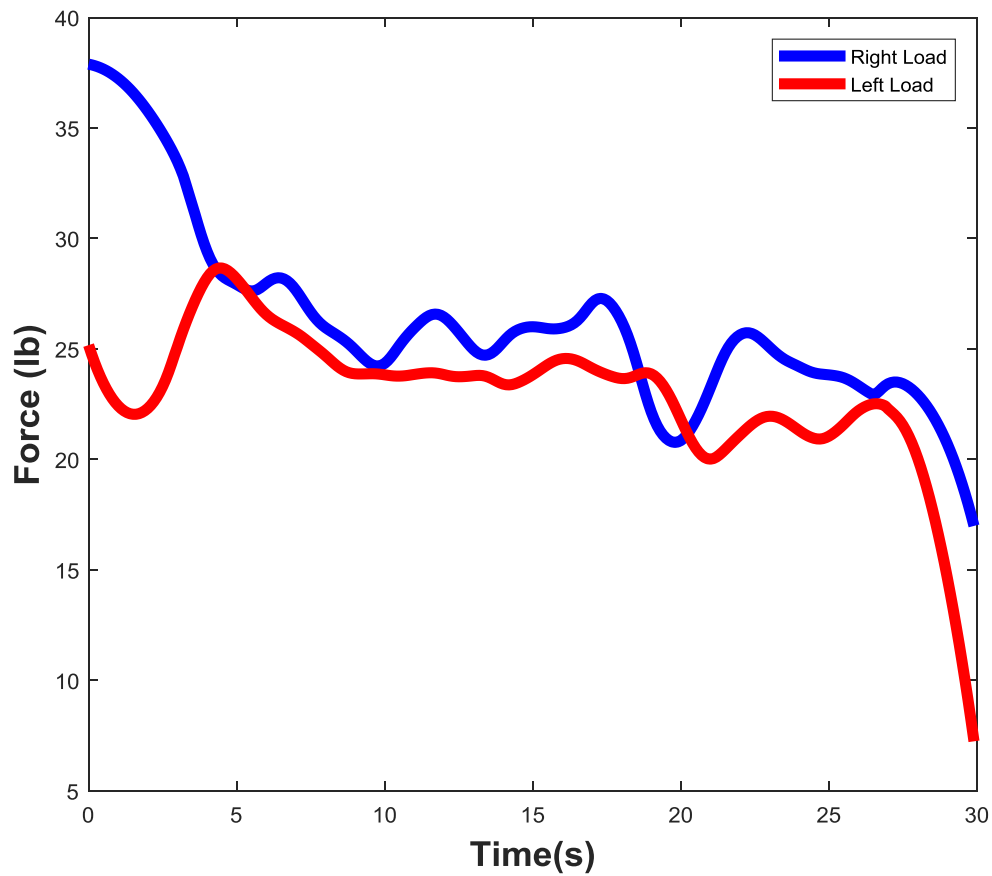


Figure 3.6: Force (lb) applied to arm rests with respect to time (s) for the test for 25% unweighting.

For the third test the subject attempted to apply 50% body weight or 90 pounds total but the maximum load they were able to start with was only about 60 pounds as shown in Figure 3.7. Furthermore, the user found that the 60 pounds was difficult to maintain for the longer duration and their arms got tired so there was a decline in load which ended at around 50 pounds total. A longer duration of 180 seconds is shown in Figure 3.7a to demonstrate the difficulty that the user had in applying the 50% unweighting. Figure 3.7b is a 30 second duration so that direct comparison to the other tests can be made.

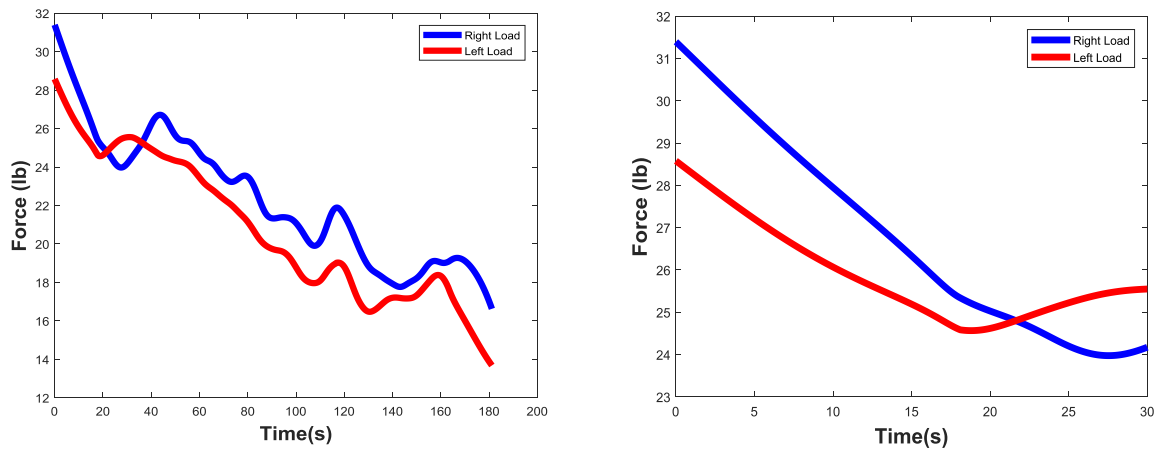


Figure 3.7: Force (lb) applied to arm rests with respect to time (s) for 50% unweighting. (a) 180 second trial (b) 30 second trial.

3.4 Inertial Measurement Unit Procedure

To operate the IMU device the black switch is pressed to turn on the IMU. The subject then attached it to their shoe as shown in Figure 3.8. Data was recoded using the smartphone application and since this was integrated as a slave device to the speed/distance module the recording was synchronized with the other modules.



Figure 3.8: IMU position for Afari use.

3.4.1 Inertial Measurement Unit Results

The foot to floor angles for the three tests are graphed in MATLAB for each test and are shown in Figure 3.9, 3.10, 3.11. When comparing these figures a similar pattern is shown in the foot to floor angle which has a peak from 20 to 30 degrees which indicates the heel strike instance and a trough varying from 40 to 60 degrees which indicates the toe-off instance. There is a slight difference in the peaks and troughs for the foot to floor angles from the different loads applied to the arm rests which will be discussed in Section 3.8.

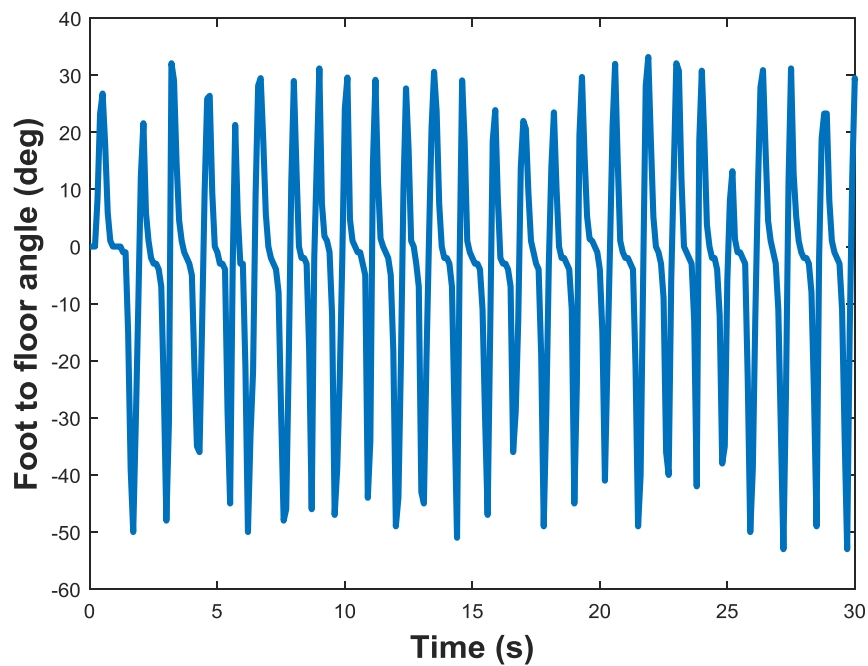


Figure 3.9: Graph of foot to floor angle (deg) with respect to time (s) for no unweighting.

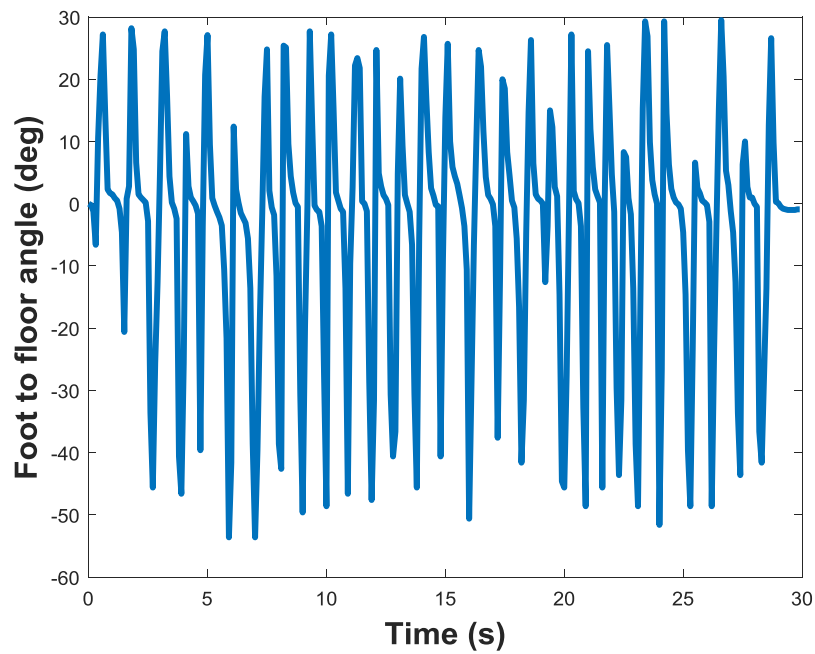


Figure 3.10: Graph of foot to floor angle (deg) with respect to time (s) for 25% unweighting.

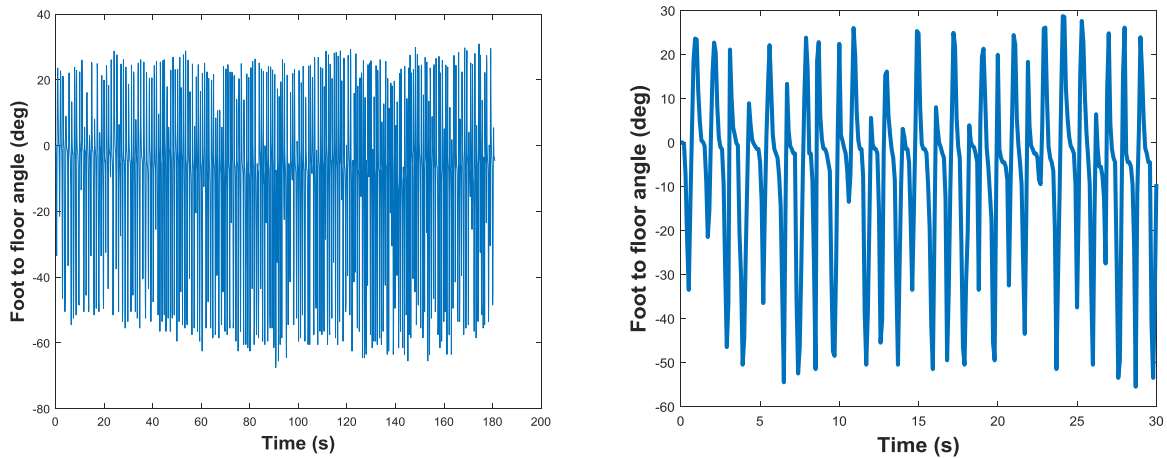


Figure 3.11: Graph of foot to floor angle (deg) with respect to time (s) for 50% unweighting (a) 180 second trial (b) 30 second trial.

The foot to floor or pitch angle's importance is to detect the heel strike and the angles of toe-off and heel strike for possible helpful clinical information described in Section 1.7. One cycle is shown in Figure 3.12 with the heel strike, zero point, and toe-off instances marked. The peaks

were detected in MATLAB with the findpeaks function to compute the cadence, step count, and heel strike angle and using this data with the distance results the stride length was also calculated. The findpeaks function was also used to find the average toe-off angles.

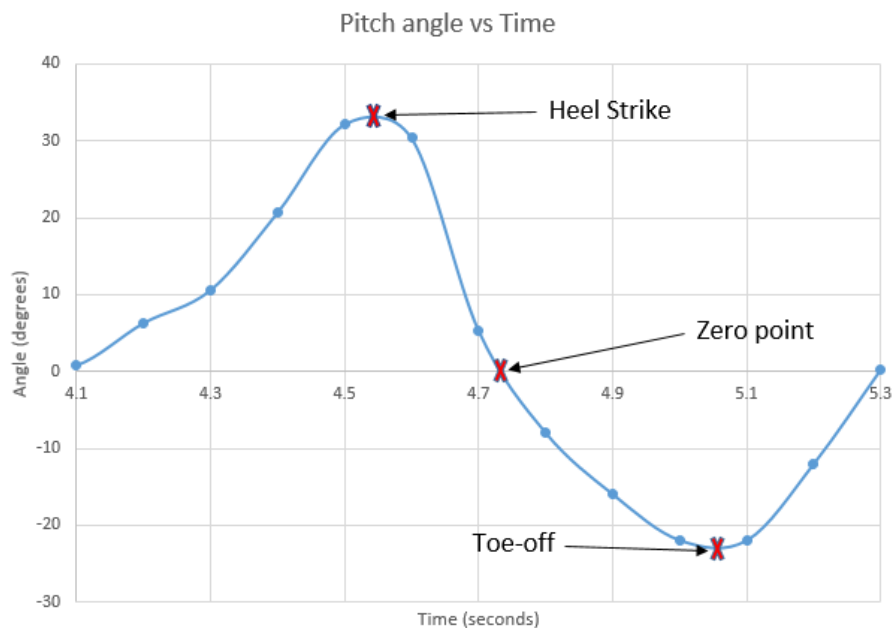


Figure 3.12: Graph of pitch angle (deg) with respect to time (s) of one stride cycle.


3.5 TekScan Procedure

While the Afari effectively measures the upper body force applied from their forearms to the arm rests, there was also interest in the lower body force applied by the subject. Accordingly, the foot sensor module is currently under development to estimate vertical ground reaction forces. To assess the value of this information a TekScan F-Scan system, that is a laboratory grade device was used. F-Scan TekScan foot pressure sensors shown in Figure 3.13 were placed inside the subject's shoe and tested while using the Afari to retrieve the force distribution of a person's feet while walking.



Figure 3.13: TekScan foot pressure sensor.

The F-Scan TekScan sensor is a grid of pressure sensors that allow for the mapping of the dynamic force of the foot. The set-up for the TekScan system involves a lot of steps and is outlined below.

1. Insert charged battery, turn on and connect to computer using A123456789 as network key.
2. Open F-Scan software and load or make new patient.
3. Click on  button in the upper right toolbar to have the software recognize the device.

Ensure both cuffs are connected, to do this connect and disconnect the device until both channels are recognized, this is shown in the Figure 3.14.

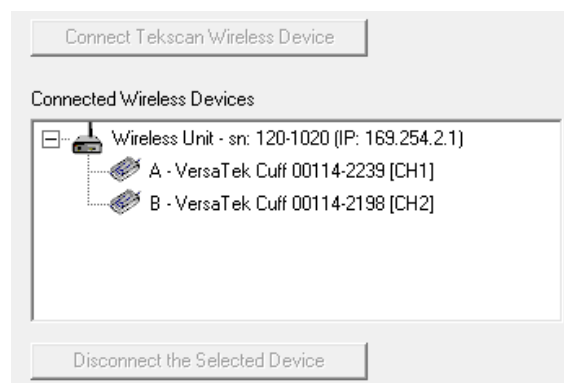



Figure 3.14: TekScan successful channel recognition

4. Calibrate the sensors by going to Tools, calibration, and either load a previous calibration or make a new one. Step calibration was used here as it was the most effective.
5. Now you can make start recording by pressing  in the toolbar or file, new recording.
6. To record a movie, press movie and record.
7. To choose the duration of recording go to options, acquisition parameters, and time and frames/second can be adjusted.
8. To view the results, press Analysis, properties, choose desired property, and then press show panes.

3.5.1 Tekscan Hardware Setup:

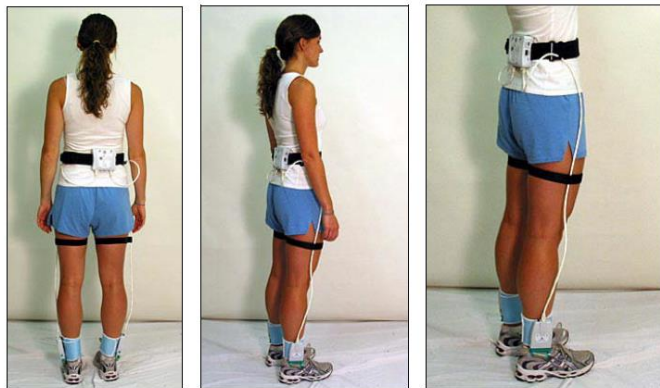


Figure 3.15: TekScan sensor system set-up (F-Scan User Manual).

1. First attach the waist strap around the subject.
2. Attach ankle bands and attach the cuffs with Velcro.
3. Finally connect cables from the cuffs to the hub on subject's waist.

3.5.2 TekScan Results

Unfortunately, the TekScan system was inconsistent and showed significant amounts of hysteresis during use. Furthermore, the sensors are delicate, and any bend can cause pressure to be artificially high in that area resulting in peaks of force or an offset that is non-zero.

Nevertheless, one of the successful trials is shown in Figure 3.16.

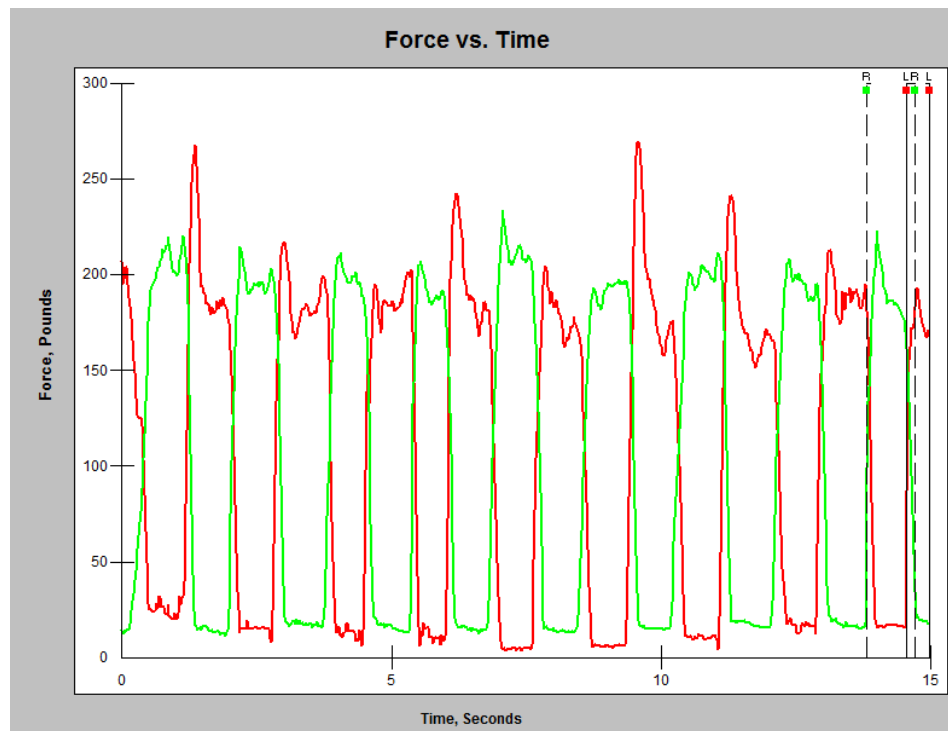


Figure 3.16: Force (lb) of each foot with respect to time (s) while walking. Red line is right foot, green line is left.

The offset for both feet is around 10.0 pounds and the right foot had peaks go as high as 250.0 pounds even though the subject's weight was only 190.0 pounds and this is due to minimal defects in the sensor. New TekScan sensors were tested as well but this problem still occurred.

3.6 Force Sensor Testing Procedure

After unsuccessful trials with the TekScan F-Scan foot pressure sensor system, the development of a custom foot pressure measurement unit, described in Section 2.1.4, was attempted. The goal was to design a foot pressure measurement unit that was more affordable, comfortable, user-friendly, and consistent than the TekScan F-Scan foot pressure sensor system which would be incorporated into the INTRAC network. The first step was to test five different force sensors purchased for under \$30 shown in Figure 3.17 a calibration rig was designed shown in Figure 3.18.

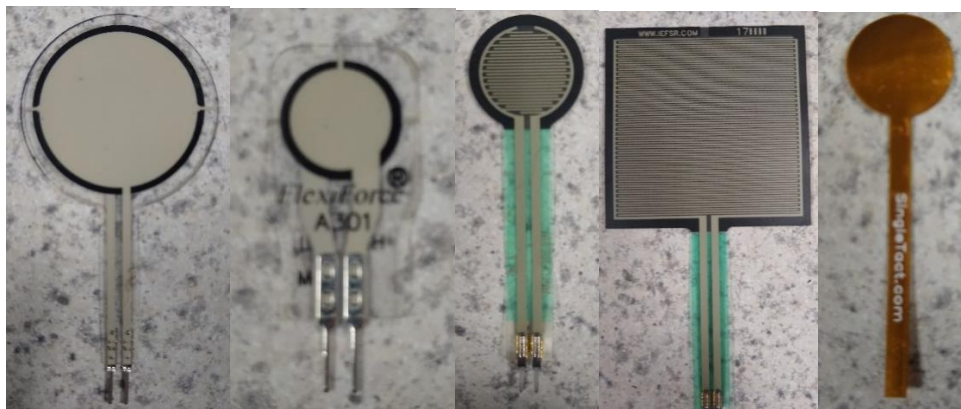


Figure 3.17: Four separate force sensors and one capacitive sensor on the far right.

These sensors include two TekScan force sensing resistors (FSRs) shown on the left, the darker FSRs in the middle are from Mouser Electronics and the sensor on the far right is a SingleTact force-sensing capacitor. The difference between a force-sensing capacitor and a force-sensing resistor is that it measures the capacitance change when a force is applied as opposed to the resistance change. These were all tested to find the one that gave the most accurate and repeatable force results of a person walking. The sensor chosen would be embedded into a molded shoe insole shown in Section 2.1.4.

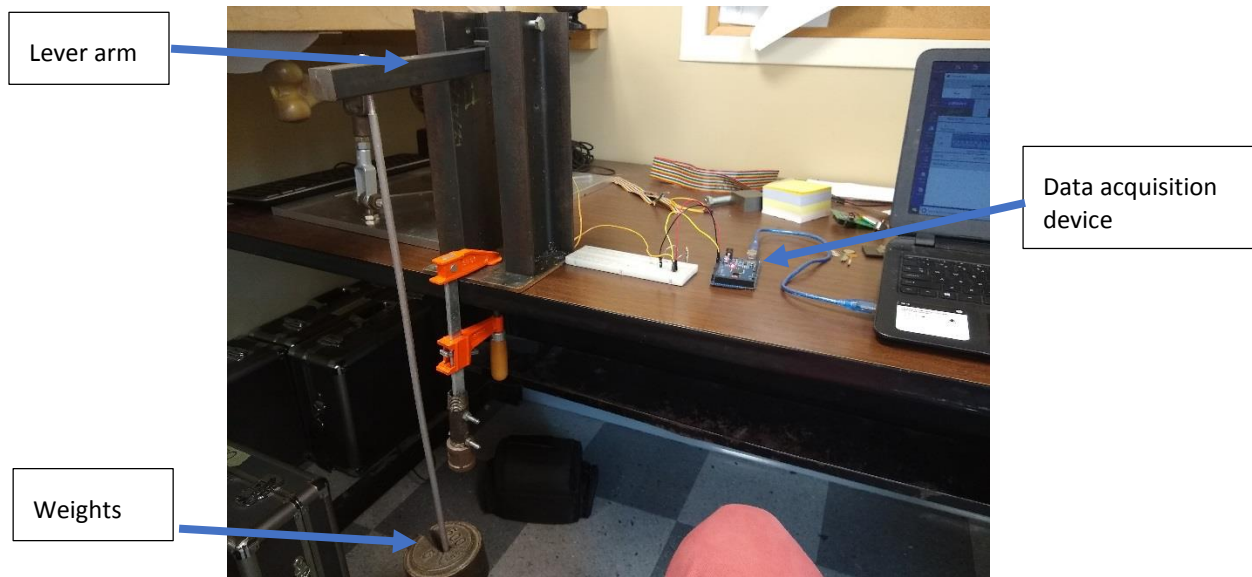


Figure 3.18: Testing set-up for calibration of force sensors.

This calibration rig applies weight to the force sensors with a lever arm that has weight attached to the end. The same routine as the load cells was used applying the weights but to test hysteresis the unweighting was also recorded. The data acquisition device is an Arduino connected to a computer and readings were taken periodically with each weight applied. Figure 3.19 has a closer look at the interaction between the force sensor and the clamp area where all the force is applied from the weights attached to the lever arm. The distance between this area and the fulcrum was 8.0 inches and the distance between the fulcrum and the applied weights was 2.0 inches which is needed to calculate the force applied between the clamp and the force sensor. This gives a ratio of $8/2$ or 4.0 so that the weight applied to the force sensor will be four times the weight attached.

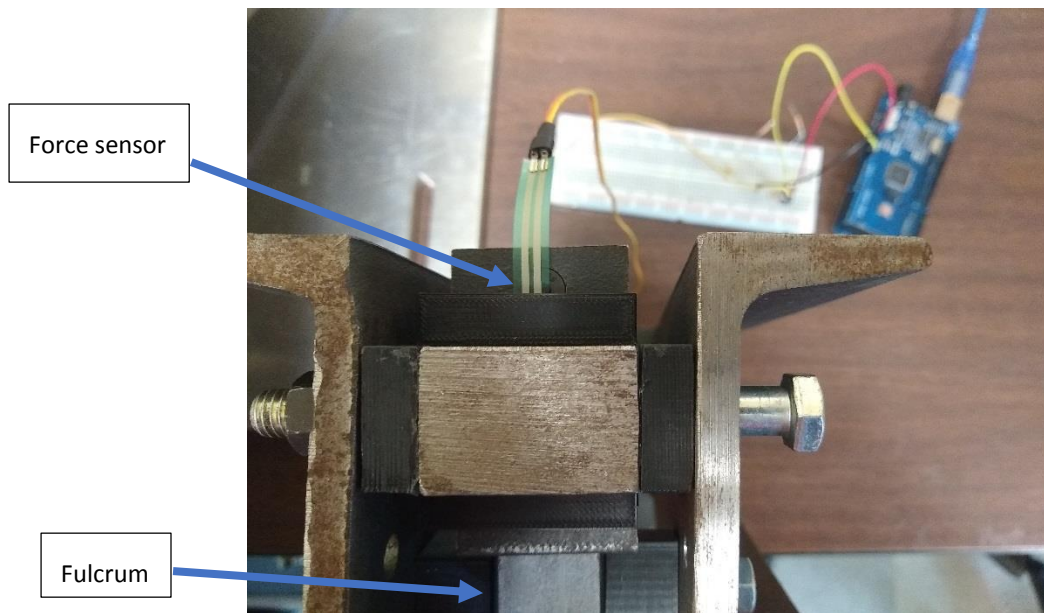


Figure 3.19: Interaction between the force sensor and clamp area.

3.6.1 Force Sensor Results

The calibrations of the Mouser Electronic FSRs was graphed in Excel and are shown in Figures 3.20 and 3.21:

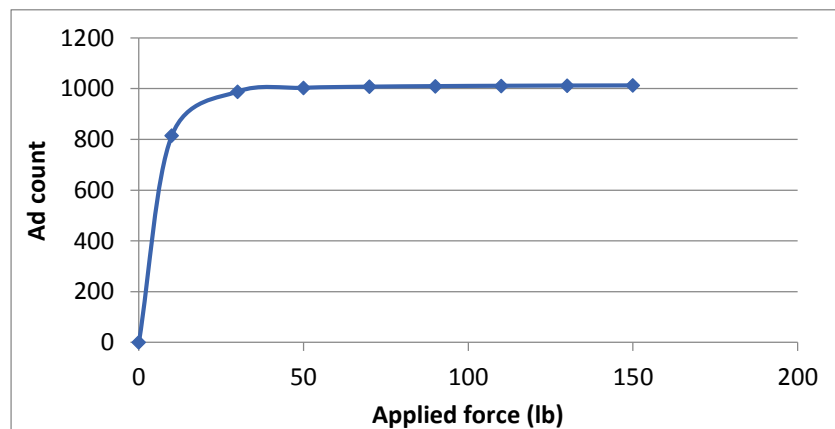


Figure 3.20: AD count with respect to applied force (lb) for Mouser Electronic rectangular FSR.

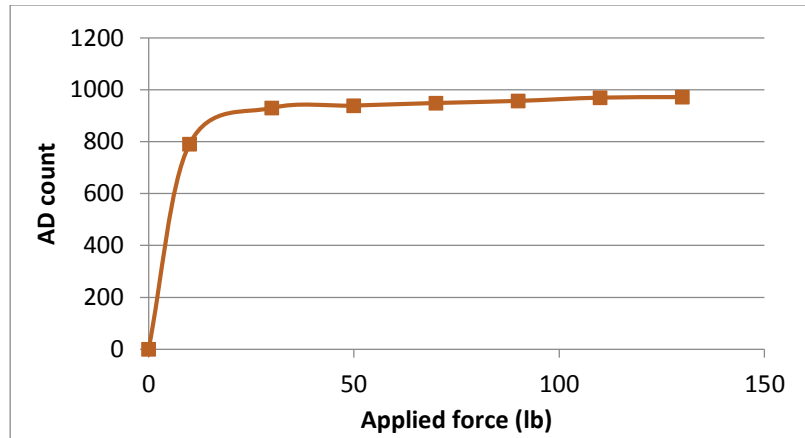


Figure 3.21: AD count with respect to applied force (lb) for Mouser Electronic circular FSR.

These sensors were abandoned because their response leveled at only 20.0 pounds which is not adequate for the weight of a person. Figures 3.22, 3.23, and 3.24 are the responses of the other three sensors that showed better results:

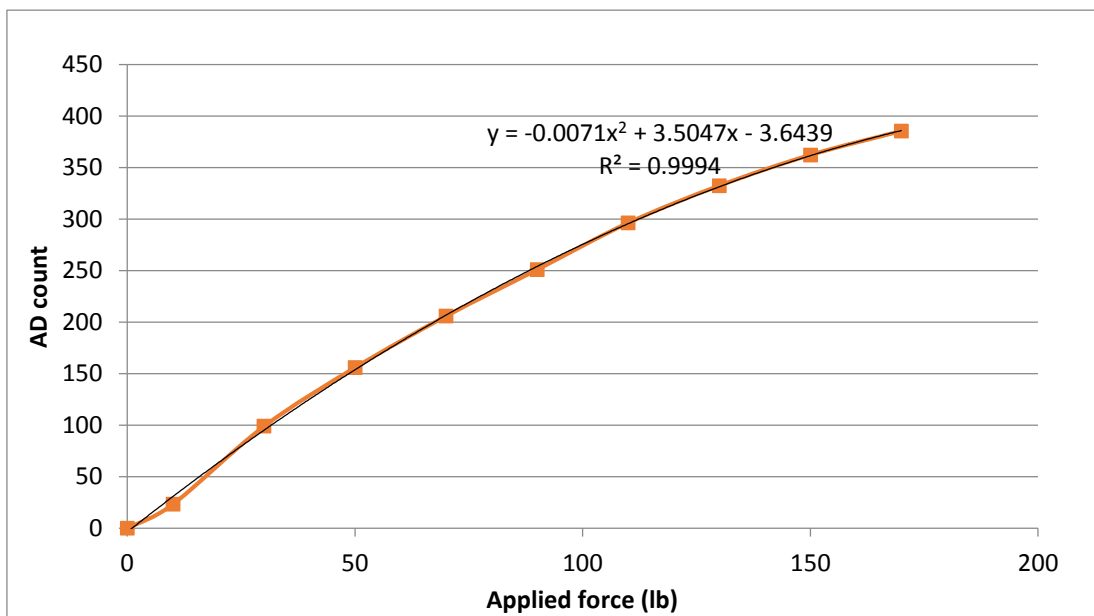


Figure 3.22: AD count with respect to applied force (lb) for TekScan large FSR response.

This data was fitted with a second order trend line and had a regression value of 0.9994.

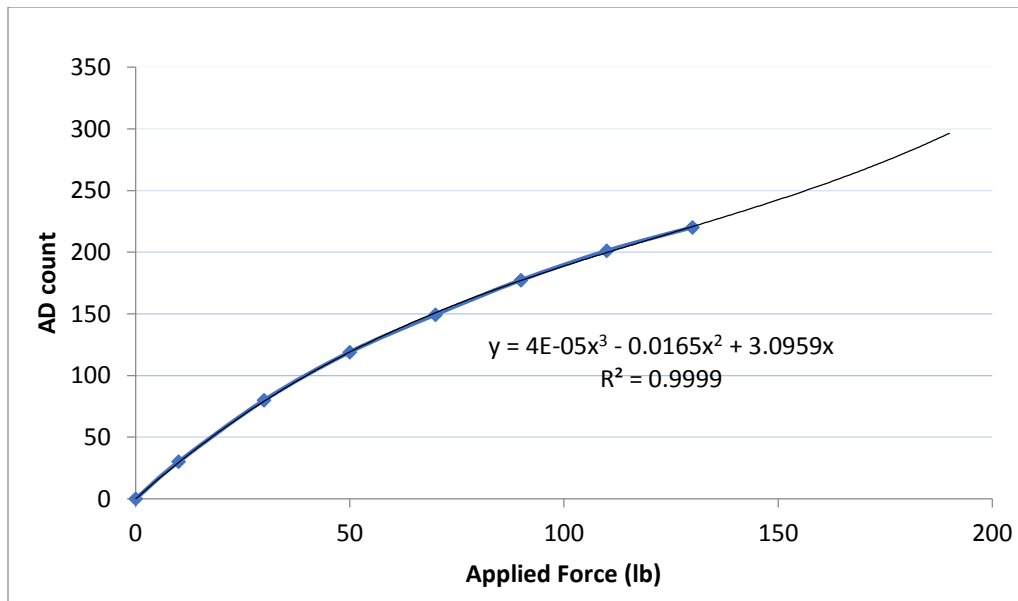


Figure 3.23: AD count with respect to applied force (lb) for TekScan small FSR

This data was fitted with a third order trend line and had a regression value of 0.9999.

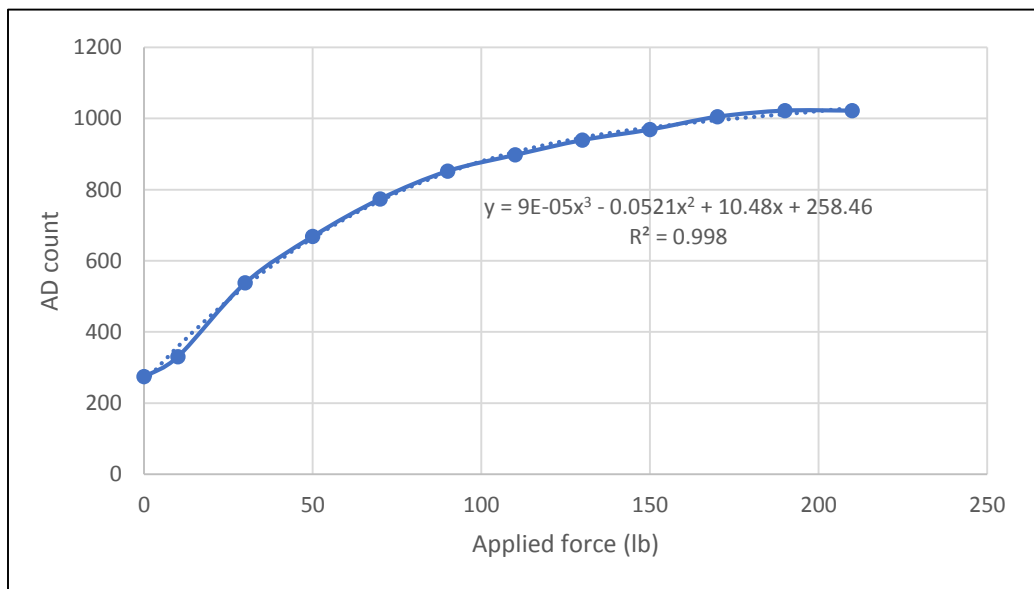


Figure 3.24: AD count with respect to applied force (lb) for SingleTact capacitive sensor response.

This data was fitted with a third order trendline and had a regression value of 0.9998.

Next the hysteresis of the two TekScan sensors and SingleTact sensor were tested to choose the best option shown in Figure 3.25.

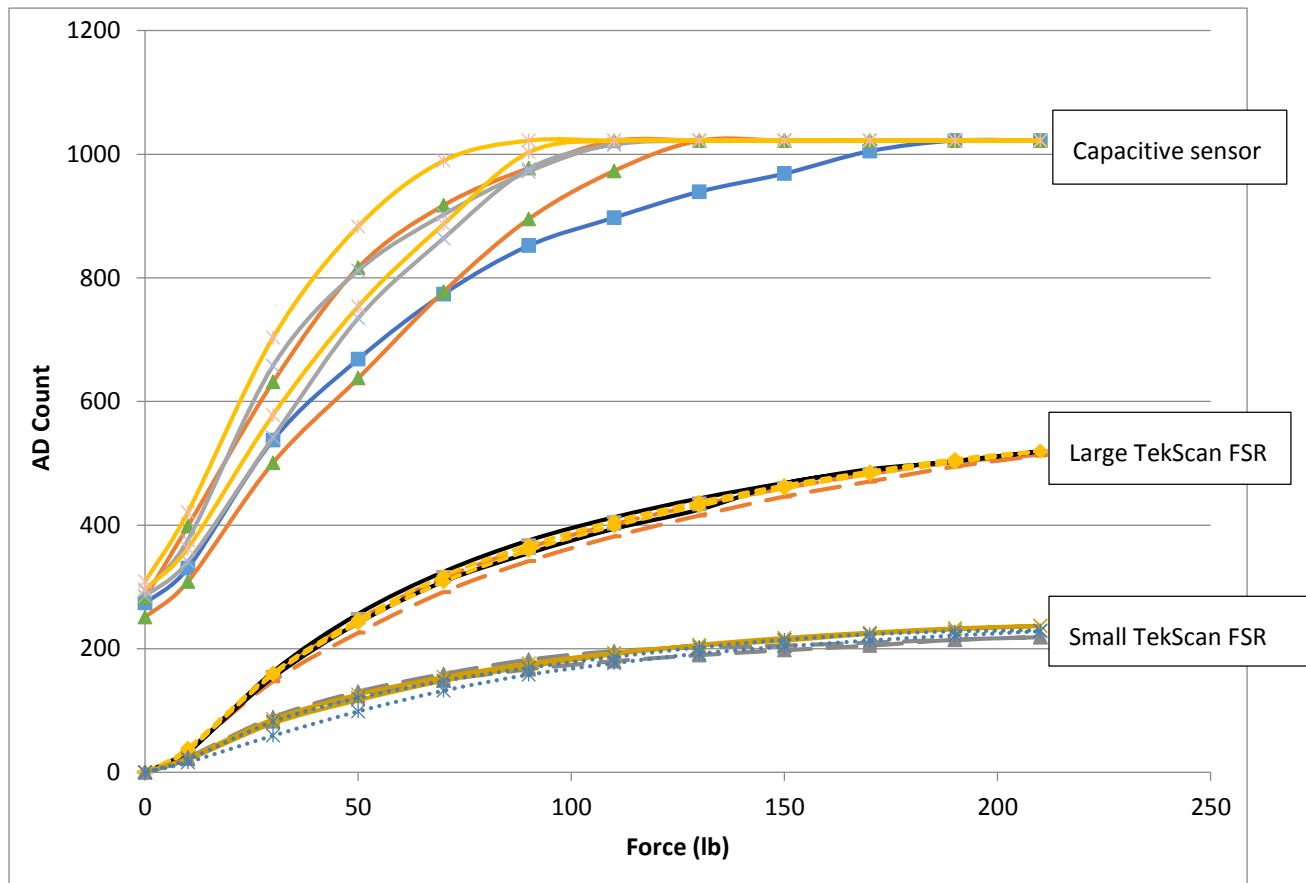


Figure 3.25: AD count with respect to applied force (pounds) for loading and unloading of the three different sensors labelled.

The hysteresis was significant for the SingleTact capacitive sensor but minimal for both the small and large TekScan FSRs. Therefore, either TekScan sensor would work effectively for measuring the force of person's foot while walking.

3.7 Data Acquisition Device

The INTRAC application has several versions coded that are compatible with Windows based computers, Android phones or I-phones. This flexibility of useable devices ensures most users with an Afari could use the activity tracking capabilities. From test trials with the computer used as a stationary data acquisition device for the Afari it has a limited range of about 30 meters due to the limits of Bluetooth 4.1 range. Therefore, a subject using the computer will need to stay within this range to capture their activity. The smartphone is the most effective device to use in tandem with the Afari as it can be placed on the handles with a phone holder and the user can see their upper body balance and distance in real time. A user could also carry the phone on them if that is preferable and take it out once finished with their activity session to view their upper body balance over time and total distance. The session's data can then be sent via e-mail so post processing be can performed to acquire additional activity information such as cadence, average heel strike angle and toe-off angle, stride length, and average speed.

3.8 System Performance Evaluation

To test all the sensors the user will need a phone to download the INTRAC application. Once it is downloaded and they have the inertial measurement unit, speed and distance sensor, and load cells attached to the Afari they will be ready to start activity tracking and monitor their progress while using the Afari. When the INTRAC application is started, the screen in Figure 3.26 will appear.

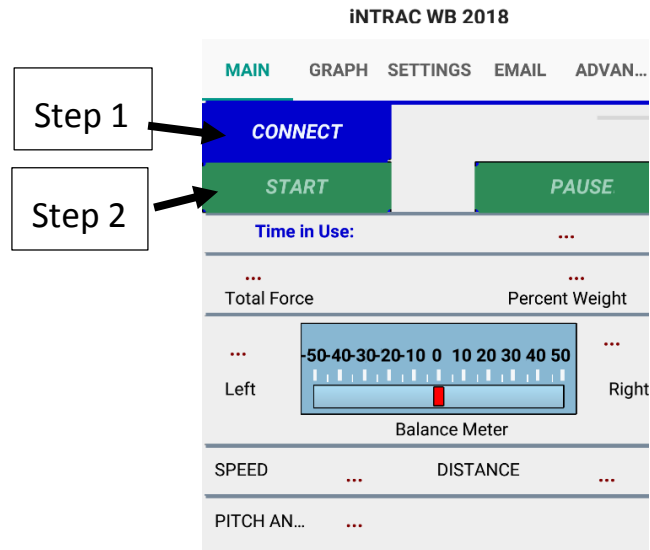


Figure 3.26: User interface of Afari application before being connected to devices; Step 1 Connect, Step 2 Start.

The first step to using this application with the Afari is to turn on all the sensors, the load cells, IMU, and the distance sensor which is the master device. The application can be run to record data solely from the IMU or load cells, but the distance sensor must be turned on to transmit the data to the phone. The IMU should be clipped to the subject's shoe so that the bottom face is parallel with the floor shown in Figure 3.4. Next the user presses the connect button labelled step 1 in Figure 3.26 and the LED of the load cells, IMU, and distance sensor will go from green to blue to signal successful connection. Finally, when all the sensors are connected the start button labelled step 2 in Figure 3.26 should be pressed and the subject can walk with the Afari. The subject can see their right and left loads from their forearms, distance, speed, and foot-to-floor/pitch angle in real time as shown in Figure 3.27.

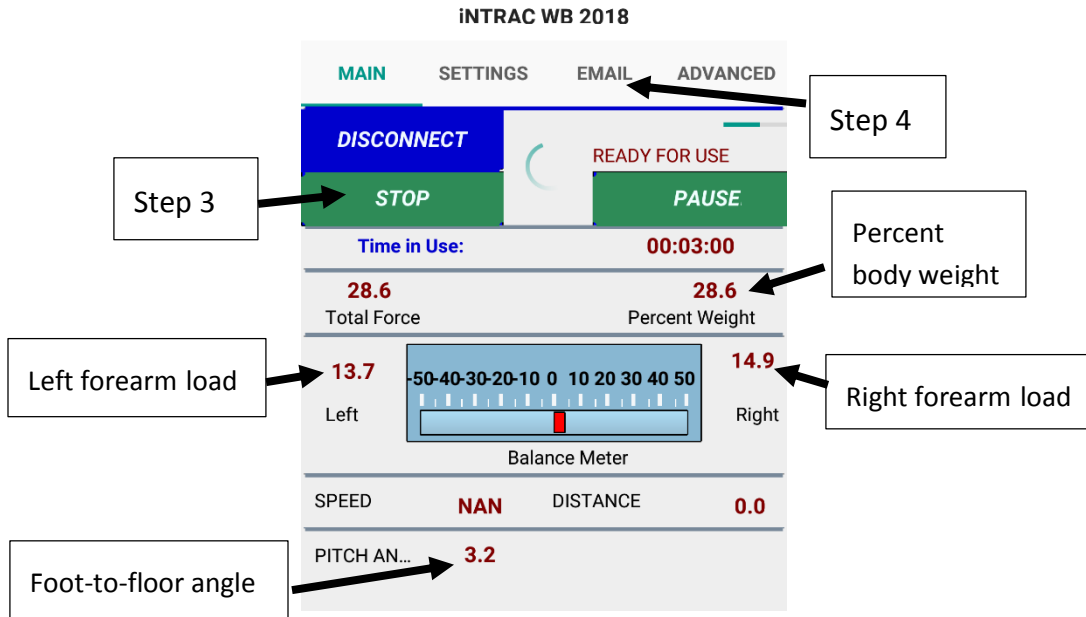


Figure 3.27: User interface of Afari application while being connected to all sensors; Step 3 Stop, Step 4 E-mail.

When the subject is finished using the Afari the stop button, labelled step 3 in Figure 3.27, needs to be pressed and the data can be transferred through the e-mail tab labelled step 4 for post-processing.

After the data loaded into the MATLAB algorithm named AFARI.m (see Appendix A), graphs of right and left load, pitch angle and distance with respect to time will be presented as shown in Sections 3.2.1, 3.3.1, and 3.4.1. Also, cadence, stride length, step count, average heel strike angles, average toe-off angle, and average speed are calculated and displayed. Sample results of the MATLAB script from the 25% unweighting test described in section 3.1 is shown on the next page and the results from all three tests are tabulated in Table 3.1.

>> AFARI

Average toe-off angle is 42.63 degrees

Average heel-strike angle is 22.84 degrees

Step count is 58.00 steps

Cadence is 116.39 steps per minute

Average speed is 1.76 mph

Average stride length is 4.16 feet

Average total load is 49.07 pounds

Furthermore, a warning message shown below will be displayed if the subject is toe-walking which is detrimental to balance increasing the chance of falling as mentioned in Section 1.7.

>> AFARI

Warning: You seem to be toe-walking, it is recommended to contact the ground with your heel first to gain stability.

Table 3.1 gives a summary of the unweighting test results for a healthy 27-year-old male using the Afari. The heel strike angle decreases as more weight is applied to the arm rests. This could be due to the fact that additional stability from the heel rocker motion, discussed in Section 1.8, is needed when the user is not unweighting as much on the Afari. Furthermore, the average speed and cadence increase when the user applies more weight to the arm rests. This may be due to the fact that the user is leaning forward more to apply the extra weight increasing the momentum of the Afari leading to a faster pace. The average stride length remains the same

for no unweighting but increases for the 50% unweighting and this could be contributed to the faster pace of this test. The average total load was 0.0 pounds for the no unweighting test as expected, 49.07 pounds for 25% unweighting test which is 4.07 pounds higher than the attempted 45 pounds, and 54.82 pounds for 50% unweighting test which is 35.18 pounds lower than the attempted 90.0 pounds which was explained in Section 3.3.1.

Table 3.1-Gait and Balance Parameters

	Test 1 0% unweighting	Test 2 25% unweighting	Test 3 50% unweighting
Average toe-off angle (deg)	46.39	42.63	49.96
Average heel-strike angle (deg)	27.67	22.84	21.42
Test period (sec)	30	30	30
Step count	54	58	60
Cadence (steps/min)	108	116	120
Average speed (mph)	1.51	1.76	2.36
Average stride length (ft)	4.16	4.16	5.02
Average total load (lb)	0.0	49.07	54.82

CHAPTER 4

SUMMARY AND CONCLUSION

The current Afari tracking system can measure a person's weight bearing, important gait characteristics, speed and distance with high accuracy. The versatility of the wireless BLE network allows for additional sensors, including the foot pressure module discussed in section 2.1.4, to be added if additional balance and gait parameters are desired. This versatility allows for sensors to be replaced as well and an alternative method for measuring speed, distance and other quantities to be implemented. For example, an alternative method for speed distance measurement would be to place an inertial measurement unit on the wheel to track its rotation with the measured angle instead of counting the magnets each time it passes the reed switch. With an IMU attached to the wheel each tenth of a degree could be measured bringing the distance resolution down to 0.023 inches as opposed to the current resolution of 4.53 inches. Other adjustments include improvements in the INTRAC software so the post processing is performed on the smartphone or computer so the gait and balance parameters are accessible immediately during use of the Afari. Eliminating the additional steps of e-mailing and loading the data into MATLAB would optimize the ease of use for activity tracking. This could be done by converting the MATLAB algorithm made for the e-mailed data files to C+ code format which could be incorporated into the INTRAC application. Furthermore, it could be beneficial for the application to store the history of each of the subject's sessions so the user could easily monitor their progression over longer periods of time.

Successful testing of the system was accomplished using a single user that attempted to run trials with 0%, 25% and 50% unweighting levels. The user was able to apply the 25%

unweighting within an acceptable margin. They were unable to consistently apply 50% unweighting. These tests also showed that average speed and cadence also increased with unweighting. These tests were done with a single user to demonstrate the operation of the INTRAC system. Human trials under an IRB are recommended with a representative group of users to quantify the benefits and performance of the device as it pertains to potential users of the Afari.

REFERENCES

1. Sijobert, Benot, et al. "Implementation and Validation of a Stride Length Estimation Algorithm, Using a Single Basic Inertial Sensor on Healthy Subjects and Patients Suffering from Parkinsons Disease." *Health*, vol. 07, no. 06, 2015, pp. 704–714., doi:10.4236/health.2015.76084.
2. University of California - Disability Statistics Center. "Mobility Device Statistics - United States." *Disabled World*, Disabled World, 18 Mar. 2015, www.disabled-world.com/disability/statistics/mobility-stats.php.

"Gait-Force Model and Inertial Measurement Unit-Based Measurements: A New Approach for Gait Analysis and Balance Monitoring." *Egyptian Journal of Medical Human Genetics*, Elsevier, 4 Nov. 2016, www.sciencedirect.com/science/article/pii/S1728869X16301538.
3. Ellis, Robert J., et al. "A Validated Smartphone-Based Assessment of Gait and Gait Variability in Parkinson's Disease." *Plos One*, vol. 10, no. 10, 2015, doi:10.1371/journal.pone.0141694.
4. Sun, Bing, et al. "Gait Characteristic Analysis and Identification Based on the iPhone's Accelerometer and Gyrometer." *Sensors*, vol. 14, no. 9, 2014, pp. 17037–17054., doi:10.3390/s140917037.
5. "Adafruit BNO055 Absolute Orientation Sensor." *Power Usage / Adafruit Motor Shield / Adafruit Learning System*, learn.adafruit.com/adafruit-bno055-absolute-orientation-sensor/overview.
6. Martinez, Monica. "RELIABILITY OF ACCELEROMETERBASED GAIT ANALYSIS: PROVIDING A BASIS FOR COMPARISON." parasol.tamu.edu/dreu2015/Martinez/FinalRep
7. Fortune, Emma, et al. *Advances in Pediatrics.*, U.S. National Library of Medicine, June 2014, www.ncbi.nlm.nih.gov/pmc/articles/PMC4030415/.
8. Resnik, Linda, et al. "Perspectives on Use of Mobility Aids in a Diverse Population of Seniors: Implications for Intervention." *Disability and Health Journal*, vol. 2, no. 2, 2009, pp. 77–85.

9. “Tips for Choosing and Using Walkers.” *Mayo Clinic*, Mayo Foundation for Medical Education and Research, 8 Sept. 2016, www.mayoclinic.org/healthy-lifestyle/healthy-aging/multimedia/walker/sls-20076469?s=7.
10. Zheng, Chong Yu, and Jasmy Yunus. “Wearable Movement Analysis System for Children with Movement Disorders - Lower Extremities Assessment System.” *IFMBE Proceedings The 15th International Conference on Biomedical Engineering*, 2014, pp. 395–398., doi:10.1007/978-3-319-02913-9_101.
11. “3-Space™ Bluetooth.” *Yost Labs*, yostlabs.com/product/3-space-bluetooth/.
12. Sándor, Zátonyi. “File:Reed Switch.ogg.” *Wikipedia*, Wikimedia Foundation, en.wikipedia.org/wiki/File:Reed_switch.ogg.
13. Vargas-Valencia, Laura, et al. “An IMU-to-Body Alignment Method Applied to Human Gait Analysis.” *Sensors*, vol. 16, no. 12, Oct. 2016, p. 2090., doi:10.3390/s16122090.
14. Chang, Alison, et al. “The Relationship between Toe-out Angle during Gait and Progression of Medial Tibiofemoral Osteoarthritis.” *Annals of the Rheumatic Diseases*, BMJ Group, Oct. 2007, www.ncbi.nlm.nih.gov/pmc/articles/PMC1994298/.
15. Vette, Albert H., et al. “The Utility of Normative Foot Floor Angle Data in Assessing Toe-Walking.” *The Foot*, vol. 37, 2018, pp. 65–70., doi:10.1016/j.foot.2018.07.003.
16. Perry, Jacquelin. “Normal Gait.” 13: Normal Gait | O&P Virtual Library, www.oandplibrary.org/alp/chap13-01.asp.
17. Cortés, U., et al. “A SHARE-It Service to Elders’ Mobility Using the i-Walker.” *Gerontechnology*, vol. 7, no. 2, 2008, doi:10.4017/gt.2008.07.02.032.00.
18. “MMR.” *MbientLab*, mbientlab.com/metamotionr/.
19. Weiss, Viviana, et al. “Walking Behavior Change Detector for a ‘Smart’ Walker.” *Procedia Computer Science*, vol. 39, 2014, pp. 43–50., doi:10.1016/j.procs.2014.11.008.

20. Postolache, O., et al. "Assistive Smart Sensing Devices for Gait Rehabilitation Monitoring." Communications in Computer and Information Science ICTs for Improving Patients Rehabilitation Research Techniques, 2015, pp. 234–247., doi:10.1007/978-3-662-48645-0_20
21. "Load Cell Vs. Force Sensor." Tekscan, 12 Mar. 2018, www.tekscan.com/resources/whitepaper/load-cell-vs-force-sensor.
22. "Strain Gauges." All About Circuits, 19 June 2019, www.allaboutcircuits.com/textbook/direct-current/chpt-9/strain-gauges/.
23. Western, D. G., et al. "Validation of Inverse Dynamics Modelling and Correlation Analysis to Characterise Upper-Limb Tremor." Converging Clinical and Engineering Research on Neurorehabilitation Biosystems & Biorobotics, 2013, pp. 697–702., doi:10.1007/978-3-642-34546-3_113.
24. Li, Xinan, et al. "Gait-Force Model and Inertial Measurement Unit-Based Measurements: A New Approach for Gait Analysis and Balance Monitoring." Journal of Exercise Science & Fitness, vol. 14, no. 2, 2016, pp. 60–66., doi:10.1016/j.jesf.2016.07.002.
25. Zhu, Shenggao, et al. "A Real-Time On-Chip Algorithm for IMU-Based Gait Measurement." Advances in Multimedia Information Processing – PCM 2012 Lecture Notes in Computer Science, 2012, pp. 93–104., doi:10.1007/978-3-642-34778-8_9.
26. BNO055 Intelligent 9-axis absolute orientation sensor Data Sheet, Bosch Sensortec, Reutlingen, Germany, 2016.
27. Yasin, Ahmad Muammar Bin Md, et al. "Design of an Assistive Walking Device with Special Rehabilitation Capabilities." Universal Journal of Mechanical Engineering, vol. 4, no. 6, 2016, pp. 147–152., doi:10.13189/ujme.2016.040603.
28. Jiménez, Mario F., et al. "Admittance Controller with Spatial Modulation for Assisted Locomotion Using a Smart Walker." Journal of Intelligent & Robotic Systems, vol. 94, no. 3-4, 2018, pp. 621–637., doi:10.1007/s10846-018-0854-0.
29. Weiss, Viviana, et al. "An Embedded Ground Change Detector for a 'Smart Walker.'" Artificial Computation in Biology and Medicine Lecture Notes in Computer Science, 2015, pp. 533–542., doi:10.1007/978-3-319-18914-7_56.

APPENDIX A

MATLAB Algorithm

```
num=xlsread('C:\Users\Lab User\Desktop\Thesis files\AFARI10hzlight.xlsx');
%Create vectors of E2 angles, right and left loads, and distance

E2=num(1:end,6);
E2=(E2(~isnan(E2)));

rightload=num(1:end,3);
leftload=num(1:end,2);
distance=num(1:end,4);

%Find standing event
stand=diff(E2);
x=find(stand==0);

%Might be necessary to create if statement in case person doesn't stand
%still

%Find time where person starts walking after standing:
start1=abs(stand(x(1):end));
startevent=find(start1>2);
u=startevent(1);

%Create angle and time vector (%t1 is set to 10 Hz but is subject to change)
%from walk start to end:

st=x(1)+u;
E2n=num(st:end,6);
l=length(E2n);
t1=(l/10)-.1;
t=0:.1:t1;

%Create distance vector from time person starts walking

startdist=num(st:end,4);

%Plot distance vs. time

Figure('Name','Distance vs. Time');

plot(t, startdist,'r-')
xlabel('Time')
ylabel('Distance (meters)')

%Create load vectors from walking start
```

```

strload=num(st:end,3);
stlload=num(st:end,2);

%Smooth load vector data

rloads=smooth(t,strload,0.2,'rloess');
lloads=smooth(t,stlload,0.2,'rloess');

%Plot right and left loads

Figure('Name','Load vs. Time');

plot(t,rloads,'b-',t,lloads,'r-')
legend('Right Load','Left Load')
xlabel('Time')
ylabel('Force (pounds)')

%Initial angle
inta=E2n(1);

%Create indicies for future calculations

r=length(t);

%Adjusted pitch angles to account for initial angle so it is zero.
for i=1:r
    E2n(i)=E2n(i)-inta;
end

[pks,Ezhs]=findpeaks(E2n,t,'MinPeakHeight',5);

Figure('Name','Pitch Angle vs. Time');

plot(t,E2n)

xlabel('Time')
ylabel('Pitch angle (degrees)')

%Find negative peaks to find toe-off angle

[npks,nEzhs]=findpeaks(-E2n,t,'MinPeakHeight',5);

%Find indicies of heelstrike to use with the distance vector.

[pk,ind]=findpeaks(E2n,'MinPeakHeight',5);

%Calculate gait characteristics, speed, and load

avgtoeoff=mean(npks);

```

```

heelstrikeangle=mean(pks);

stepcount=length(Ezhs).*2;

cadence=(stepcount/t(end))*60;

avgspeed=distance(end)/t(end);

hstimes=nEzhs;

avgrightload=mean(strload);

avgleftload=mean(stlload);

totalavgload=avgrightload+avgleftload;

%Stride length calculation

%Create vector of distances at each heelstrike
stridedist=startdist(ind);
%Create vector of distances between each heel strike ie stride
%length.
stridelengths=diff(stridedist);
%Calculate average stride length.
avgstride=mean(stridelengths);
%Calculate standard deviation of stride lengths.
stridedev=std(stridelengths);

formatSpec1 = 'Average toe-off angle is %4.2f degrees\n';
formatSpec2 = 'Average heel-strike angle is %4.2f degrees\n';
formatSpec3 = 'Step count is %4.2f steps\n';
formatSpec4 = 'Cadence is %4.2f steps per minute\n';
formatSpec5 = 'Average speed is %4.2f meters/second\n';
formatSpec6 = 'Average stride length is %4.2f meters\n';
formatSpec7 = 'Average total load is %4.2f pounds\n';

fprintf(formatSpec1,avgtoeoff)

fprintf(formatSpec2,heelstrikeangle)

fprintf(formatSpec3,stepcount)

fprintf(formatSpec4,cadence)

fprintf(formatSpec5,avgspeed)

fprintf(formatSpec6,avgstride)

fprintf(formatSpec7,totalavgload)

```

BIOGRAPHY OF THE AUTHOR

Drew Browning was born in Malden, Massachusetts on May 27, 1992. He was raised in Haverhill, Massachusetts, moved to Mount Desert Island, Maine when he was 14 and graduated from Mount Desert Island High School in 2010. He attended Boston University and graduated in 2014 with a Bachelor of Science degree in Mechanical Engineering. He returned to Maine and entered the Mechanical Engineering graduate program at The University of Maine in the fall of 2016. Drew is a candidate for the Master of Science degree in Mechanical Engineering from the University of Maine in August 2019.